# A STUDY OF THE EFFECT OF THE MORPHOLOGY ON THE PHOTOCATALYTIC ACTIVITY OF WO₃

## Dávidné Nagy[a], Tamás Firkala[b], Xianfeng Fan[a] and Imre Miklós Szilágyi [b,c]*

The photocatalytic activity of hexagonal (h-) WO₃ nanoparticles (NPs) and nanowires (NWs) was investigated and compared with the performance of monoclinic (m-) WO₃ nanoparticles in the aqueous photo-bleaching reaction of methyl orange (MO) under UV irradiation. It has been known that the m-WO₃ is better photocatalyst than the h-WO₃, but due to the advantageous morphology we investigated whether the h-WO₃ NWs can reach the photo-efficiency of the m-WO₃ NPs. The h-WO₃ was successfully synthesized in NW and NP morphology using a microwave (MW) assisted hydrothermal procedure starting from Na₂WO₄ and thermal annealing of hexagonal ammonium tungsten bronze (HATB), (NH₄)₀.₃₃₋ₓWO₃, respectively. We found that the h-WO₃ NWs exhibited almost three times higher photoactivity than the h-WO₃ NPs. The improved performance of the NWs can be attributed to the enlarged surface area and the good charge carrier ability of the nanowire morphology. The catalytic tests also confirmed that the morphological effect could lead to as high photoactivity in the case of h-WO₃ NWs as exhibited by the m-WO₃ NPs.

\* Corresponding Authors
    FAX: +36-1-4633408
    Email: imre.szilagyi@mail.bme.hu
[a]    University of Edinburgh, The King's Buildings, Mayfield Road, Edinburgh, EH9 3JL,UK
[b]    Budapest University of Technology and Economics, Department of Inorganic and Analytical Chemistry, Szent Gellért tér 4., Budapest, H-1111, Hungary
[c]    MTA-BME Research Group of Technical Analytical Chemistry, Szent Gellért tér 4., Budapest, H-1111, Hungary

## Introduction

In the last few decades much attention has been attracted by alternative energy resources including renewable and nuclear fusion energy due to the limitation of availability of fossil fuel on the earth. Exploiting solar light for future energy is one of the highly studied possibilities as it can provide environmental friendly and renewable source of energy. Photocatalysts are able to convert solar energy into chemical energy which can be used for numerous purposes like generation of hydrogen fuel through water splitting; purification of different aqueous media; green synthesis of various chemicals.[1]

TiO₂ was historically the first photocatalyst and still remained one of the most efficient photocatalysts under UV light. However, the large band gap energy of TiO₂ makes its application in solar photocatalysis insufficient. An option to develop solar sensitive photocatalyst is to couple TiO₂ with other semiconductors, which absorb in the Vis range. As a beneficial consequence of making composites with TiO₂, delayed recombination of the photo-generated charges can be provided. The electrons and holes can be effectively separated in the different semiconductor layers resulting in higher photo-efficiency. Narrow band gap semiconductors like WO₃, V₂O₅, Bi₂O₃ are usually considered to form a heterojunction with TiO₂.[2-4]

WO₃ attracted much attention recently, owing to its broad application prospective and advantageous chemical and electrical properties.[4,5] WO₃ is a good candidate for the fabrication of solar response photocatalyst with TiO₂ as it has absorption in the Vis range.[6] The photocatalytic activity depends on many factors, and numerous attempts were made in order to control the size distribution and the dimensionality of the nanocatalysts, because these are considered as key parameters in affecting their photocatalytic performance.[7-10] Various morphologies have already been achieved including nanotrees, nanorods, nanospheres etc.[9,11,12] Unexpectedly, it was recently reported that despite their high specific surface area in some cases certain WO₃ particles showed lower photo-efficiency.[13] The peculiar finding was accounted for the facilitated charge recombination which surpassed the positive effect of the enlarged surface area. It is also known that the crystalline phase and the composition of WO₃ play an important role in the photo-efficiency. It was revealed that usually m-WO₃ possesses better photocatalytic ability than h-WO₃.[14]

Considering these factors, in this study we aimed to investigate the overall effect of the morphology on the photocatalytic performance of different polymorphs of WO₃, with the pronounced future objective to fabricate solar active nanocomposites by coupling WO₃ polymorphs with TiO₂.

## Experimental

H-WO₃ nanoparticles were prepared by thermal annealing of hexagonal ammonium tungsten bronze (HATB), (NH₄)₀.₃₃₋ₓWO₃ at 470 °C in air.[15] H-WO₃ NWs were obtained in a microwave (MW) assisted hydrothermal synthesis at 160 °C.[5]

The reaction mixture was prepared from sodium tungstate dihydrate ($Na_2WO_4 \cdot 2H_2O$), ammonium sulphate (($NH_4)_2SO_4$), HCl and distilled water followed by the MW process in a Synthos 3000 Anton Paar reactor. After the synthesis the nanocrystals were centrifuged, washed with water and ethanol and finally dried at 80 °C for 24 h. For the preparation of the m-WO₃ NPs, $(NH_4)_{0.33-x}WO_3$ was annealed at 600 °C in air.[15]

The morphology of the as-prepared catalysts was investigated by TEM, and the images were collected by a FEI Morgagni 268D instrument. The determination of the crystalline phase of the WO₃ photocatalysts was confirmed both XRD and Raman spectroscopy. The XRD measurements were carried out by a PANalytical X'pert Pro MPD X-ray diffractometer using Cu Kα radiation. Whereas the Raman spectra were obtained by a Jobin-Yvon Labram type Raman spectrometer coupled with an Olympus BX-41 microscope. An Nd-YAG laser with a wavelength of 532 nm was applied as a light source in the Raman spectrometer. The specific surface area was determined by applying the BET model based on the absorption isotherm of nitrogen at 77 K using NOVA 2000E equipment (Quantachrome, USA).

The photocatalytic activity was measured in aqueous methyl orange (MO) (10 mg/350 ml) solution under UV irradiation. In a typical test 100 mg catalyst powder was suspended in the MO solution. The photo-reactor was a cylindrical glass reactor equipped with a Heraeus TQ 150 mercury immersion lamp. The solution was stirred and oxygen bubbling was provided. Room temperature was maintained by circulating cold water in the jacket of the photo-reactor. The concentration of MO was followed by a Jasco V-550 type UV-Vis spectrophotometer at 465 nm.

## Results and Discussion

The XRD analysis confirmed that microwave assisted hydrothermal synthesis and annealing of HATB at 470 °C in air lead to the formation of hexagonal phase WO₃ (33-1387) with no crystalline impurities present in the diffractogram. The thermal annealing process of HATB at 600 °C in air resulted in the formation of monoclinic phase WO₃ (43-1035) as confirmed by the XRD pattern.
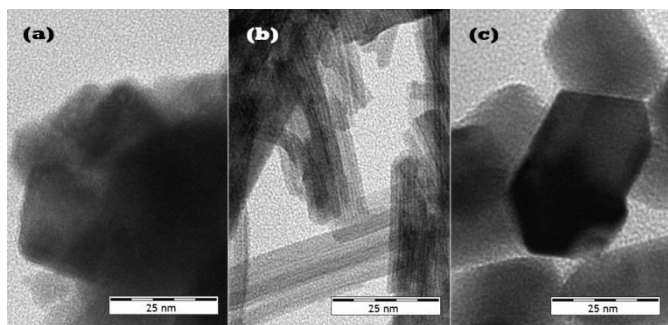


**Figure 1.** TEM images of (a) h-WO₃ NPs; (b) h-WO₃ NWs; (c) m-WO₃ NPs.

The morphology of the nanostructures was confirmed by TEM (Figure 1). The images revealed that the h-WO₃ NWs had diameters between 5 and 10 nm and were several

hundred nm long. The h-WO₃ NPs consisted of 50-70 nm particles, while the m-WO₃ NPs were made up by 60-90 nm particles.

The BET specific surface area of the h-WO₃ NP and NW was found to be 11 $m^2g^{-1}$ and 101 $m^2g^{-1}$, respectively. The nanowire morphology resulted in one order of magnitude higher specific surface area, compared to that of the nanoparticle.[14]

The Raman spectra were in good agreement with the literature and with the XRD analysis and confirmed the hexagonal and monoclinic crystalline phase of the WO₃ nanostructures.[14]
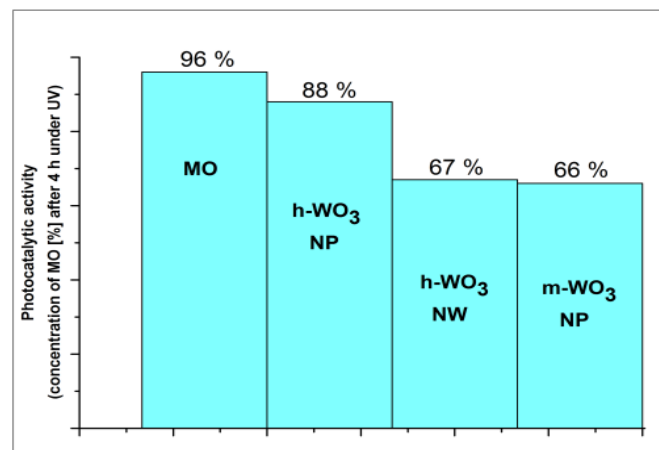


**Figure 2.** MO concentrations given in percentage after 4 hour UV irradiation in the photocatalytic test reaction.

In the photocatalytic test we found that the h-WO₃ NWs were almost three times more effective in the degradation of MO than h-WO₃ NPs (Figure 2). By the end of the 4 h UV irradiation, 12 % of the initial MO was decomposed by the h-WO₃ NPs, while the h-WO₃ NWs photo-bleached 33% of the original concentration of MO. The remarkable improvement in the photocatalytic activity could be attributed to the beneficial morphology of the h-WO₃ NWs. The findings also confirmed how important the precise control is over the morphology. The nanowire structure can provide better carrier transport to the separated charges and possess higher specific surface area leading to triple efficiency. The performance of h-WO₃ NWs was compared with the activity of m-WO₃ NPs as well. It was concluded that by the end of the photocatalytic test the h-WO₃ NWs were even more efficient (34 % MO decomposed) than the nanoparticles of the inherently better photocatalyst m-WO₃ (33 % MO decomposed). This finding revealed that the h-WO₃, which attracted much interest due to its unique open-tunnel structure, can also achieve similarly high photon efficiency as m-WO₃.

## Conclusions

In this study we successfully synthesized h-WO₃ both with NW and NP morphology along with m-WO₃ with NP nanostructure, either by a MW assisted hydrothermal synthesis route or by annealing $(NH_4)_{0.33-x}WO_3$. The crystal phase of the nanostructures was confirmed by Raman spectroscopy while the microstructures were investigated by

TEM. The morphological effect on the photo-efficiency of the synthesized h- and m-WO₃ nanostructures was elucidated. The photoactivity of the h-WO₃ NWs was almost three times higher compared to that of the h-WO₃ NPs. The significant improvement in the photo-efficiency clearly indicated the positive effect of the high aspect ratio of the NWs, which could provide more enhanced carrier transport in the photocatalytic reaction than the NP nanostructure. We also examined the question whether the h-WO₃ NWs can exhibit as high photoactivity as the m-WO₃ NPs, which have been otherwise considered to be better photocatalysts. It was found that by the degradation test the h-WO₃ NWs surpassed even the performance of m-WO₃ NPs to a small extent.

## Acknowledgements

## References

[1]Mills, A., Le Hunte S., *J. Photochem. Photobio. A,* **1997,** *108,* 1.

[2]Wojtyła, S., Baran, T., *Eur. Chem. Bull.,* **2015,** *4,* 260.

[3]Wang, Y., Wang, Y., Zhang, J., Liu, L., Zhua, C., Liu, X., Su, Q., *Mater. Lett.,* **2012,** *75,* 95.

[4]Szilágyi, I. M., Heikkilä, M., Pore, V., Kemell, M., Nikitin, T., Teucher, G., Firkala, T., Khriachtchev, L., Räsänen, M., Ritala, M., Leskelä, M., *Chem. Vapor Dep.,* **2013,** *19,* 149.

[5]Arutanti, O; Ogi, T., Nandiyanto, A.B.D., Iskandar, F., Okuyama, K., *AIChE J.,* **2014,** *60,* 41.

[6]Phuruangrat, A., Ham, D. J., Hong, S. J., Thongtem, S., Lee, J. S., *J. Mater. Chem.,* **2010,** *20,* 1683.

[7]Xu, Z., Tabata, I., Hirogaki, K., Hisada, K., Wang, T., Wang, S., Hori, T., *Mater. Lett.,* **2011,** *65,* 1252.

[8]Han, X; Han, X., Li, L., Wang, C., *New. J. Chem.,* **2012,** *36,* 2205.

[9]Zhang, J., Wang, X. L., Xia, X. H., Gu, C. D., Tu, J. P., *Sol. Energ. Mater. Sol. Cell.,* **2011,** *95,* 2107.

[10]Wang, X., Meng, X., Zhong, M., Wu, F., Li, J., *Appl. Surf. Sci.* **2013,** *282,* 826.

[11]Van Tong, P., Hoa, N. D., Quang, V. V., Van Duy, N., Van Hieu, N., *Sens. Actuat. B,* **2013,** *183,* 372.

[12]Li, J., Zhao, Q. L., Zhang, G. Y., Chen, J. Z., Zhong, L., Li, L., Huang, J., Ma, Z., *Solid State Sci.,* **2010,** *12,* 1393.

[13]Amano, F., Ishinaga, E., Yamakata, A., *J. Phys. Chem. C,* **2013,** *117,* 22584.

[14]Szilágyi, I. M., Fórizs, B., Rosseler, O., Szegedi, Á., Németh, P., Király, P., Tárkányi, G., Vajna, B., Varga-Josepovits, K., László, K., Tóth, A. L., Baranyai P., Leskelä, M., *J. Catal.* **2012,** *294,* 119.

[15]Szilágyi, I. M., Madarász, J., Pokol, G., Király, P., Tárkányi, G., Saukko, S., Mizsei, J., Tóth, A. L., Szabó A., Varga-Josepovits, K., *Chem. Mater.,* **2008,** *20,* 4116.

# REMEDIAL STUDY OF IRON INDUSTRY EFFLUENTS USING REVERSE OSMOSIS TECHNOLOGY

## A. Pandia Rajan[a,b] and M. S. Dheenadayalan[b]*

**Keywords:** Iron industry; effluent treatment; reverse osmosis

Reverse osmosis (RO) system has been effectively applied on a large scale throughout the world for the treatment of effluent and the polluted water. The Arab countries and some other affluent countries have the credit of successfully running such large scale plants without minding for the cost factor involved in such projects. Here the polluted effluent is treated using RO technology in order to remove the pollutants. The investigator has taken an attempt has been made to find out in the impact of Iron Industry Effluent and also to know about the quality of Iron Industry effluents after the treatment of using R O plant. Reverse osmosis has been successfully applied on a large scale for the treatment of effluent and the polluted water. In the present study the Iron Industry effluent are treated using RO plant and treatment can be recommended to all Iron Industries. The same reverse osmosis method can also be applied to other industry effluent.

* Corresponding Authors
    Tel: 9380939942.
    E-Mail: dr.msdchem@gmail.com
[a]    Research & Development Centre, Bharathiar University, Coimbatore, India
[b]    P.G. and Research Department of Chemistry, G.T.N Arts College, Dindigul

## INTRODUCTION

Since the development of the first practical cellulose acetate membranes in the early 1960's and the subsequent development of thin-film, composite membranes, the uses of reverse osmosis have expanded to include not only the traditional desalination process but also a wide variety of wastewater treatment applications.

RO systems are inorganic and organic pollutants can be removed simultaneously by RO membrane processes. RO processes can considerably reduce the volume of waste streams so that these can be treated more efficiently and cost effectively by other processes such as incineration. In addition, RO systems can replace or be used in conjunction with others treatment processes such as oxidation, adsorption, stripping, or biological treatment to produce a high quality product water that can be reused or discharged.[1-6]

Reverse osmosis has been successfully applied on a large scale throughout the world for the treatment of effluent and the polluted water. The Arab countries and some other affluent countries have the credit of successfully running such large scale plants without minding for the cost factor involved in such projects. Here the polluted effluent is treated using RO technology in order to remove the pollutants.[7-9]

Applications that have been reported for RO processes include the treatment of organic containing wastewater, wastewater from electroplating and metal finishing, pulp and paper, mining and petrochemical, textile, and food processing industries, radioactive wastewater, municipal wastewater, and contaminated groundwater.[1,6,10,11]

## MATERIALS AND METHODS

An attempt has been made to analyse the extent of water pollution by analyzing various water quality parameters for iron industry effluent. The effluent water sample was analysed and compared with the guideline of Bureau of Indian Standards (BIS) limit for drinking water standards. Analysis of physico-chemical characteristics of water samples were undertaken to find the water quality.

**Table 1.** Analysis of the Water Quality Parameters

| Parameter | Method of Analysis |
|---|---|
| Colour | Visual comparison |
| Turbidity | Neplo turbidimetry |
| TDS | Conductivity measurement |
| Electrical conductivity | Conductivity measurement |
| pH | pH measurement |
| Total hardness | EDTA titrimetry |
| Calcium and magnesium | EDTA titrimetry |
| Iron | Spectrophotometry |
| Ammonia | Nessler's method |
| Nitrite and nitrate | Spectrophotometrs |
| Chloride | Silver nitrate |
| Fluoride | Colorimetry |
| Sulphate | Turbidity method |
| Phosphate | Spectrophotometry |

**Reverse osmosis**

To affect a reverse process of osmosis, a pressure is applied in excess of the osmotic pressure to the concentrated solution. Now the flow is reversed from the concentrated solution to the dilute solution. It is "reverse osmosis". It is always remembered that, whether it is osmosis or reverse osmosis only the flow of water take place from one side to the other side. It is because the semi permeable membrane can allow only smaller molecules like that of water to pass through it.

**Table 2.** Working of reverse osmosis treatment plant

| FILTRATION | MATERIAL | BENEFIT |
|---|---|---|
| Pre-filter | Polypropylene yarn wound | Removes suspended particles |
| Sediment filter | Polypropylene melt blown | Removes suspended particles |
| Pre-RO carbon cartridge | Silver impregnated activated carbon | Removes excess chlorine and organic impurities |
| Reverse osmosis | Thin film composite (TFC) (0.0001 micron) | Reduces TDS, hardness, pesticides, heavy metals like arsenic, lead and mercury. Removes micro organisms like bacteria, virus and protozoa cysts. |
| Post-RO carbon cartridge | Silver impregnated activated carbon | Inhibits growth of bacteria, removes residual organic impurities and revives the original taste of water. |

**Table 3.** Physico-chemical analysis of the iron industry effluent before and after the treatment using RO system.

| Physical Parameters | BIS-Standards | Iron industry effluent analysis (S-1) | Iron industry effluent after treatment with RO system (S-2) |
|---|---|---|---|
| Appearance | _- | blackish | clear |
| Odour | nil | bad smell | colorless |
| Turbidity % NT Units | 1 | 540 | 4 |
| Total dissolved solids mg $L^{-1}$ | 500 | 6903 | 129 |
| Electrical conductivity, $\mu ohm^{-1} cm^{-1}$ | - | 10412 | 320 |
| pH | 6.5-7.5 | 6.53 | 7.57 |
| Alkalinity Ph | _ | 0 | 0 |
| Total Hardness as $CaCO_3$ ppm | 200 | 940 | 70 |
| Calcium as Ca ppm | 75 | 268 | 16 |
| Magnesium as Mg ppm | 30 | 211 | 11 |
| Sodium as Na mg $L^{-1}$ | - | 1600 | 12 |
| Iron Total as Fe mg $L^{-1}$ | 0.1 | 3.49 | 0.07 |
| Ammonia as $NH_3$ mg $L^{-1}$ | - | 0.18 | 0.09 |
| Potassium as K mg $L^{-1}$ | - | 360 | 2 |
| Nitrite as $NO_2$ mg $L^{-1}$ | - | 0.3 | 0.01 |
| Nitrate as $NO_3$ mg $L^{-1}$ | - | 54 | 5 |
| Chloride as CI mg $L^{-1}$ | 200 | 2900 | 42 |
| Sulphate on $SO_4$ mg $L^{-1}$ | 200 | 313 | 4 |
| Fluoride as F mg $L^{-1}$ | 1 | 2.6 | 0.4 |
| Phosphate as $PO_4$ mg $L^{-1}$ | - | 5.25 | 0.06 |
| Tidly's Test 4 h as $O_2$ | - | 1.53 | 0.12 |

## RESULTS AND DISCUSSIONS

The results of the various physico-chemical analysis of the iron industry effluent before and after the treatment using RO plant and the effluents samples were collected at the study area. The iron industry effluent analysis reveals that all the parameters are above the standard limit as per BIS standards.

### The iron industry effluent after treatment with reverse osmosis

The Turbidity is 4 NTU where as the standard as per BIS shows the acceptable limit is 1 NTU. The total dissolved solid value is 129 mg $L^{-1}$, which lies below the acceptable limit 500 mg $L^{-1}$. The amount of Iron is 0.07 mg $L^{-1}$, which lies below the acceptance limit 0.1 mg $L^{-1}$. For Nitrate the permissible limit is nil but the observed value is 5 mg $L^{-1}$. For Phosphate also the permissible limit is nil. But the observed value is 0.06 mg $L^{-1}$. So this water is unfit for drinking. The amount of Chloride is 42 mg $L^{-1}$ which lies below in the acceptable limit 200 mg $L^{-1}$. The permissible limit for ammonia is nil. But the observed value of the sample of water is 0.09 mg $L^{-1}$. So the water is unfit for drinking.

## CONCLUSION

The effect of chemicals in the industrial effluents affects cultivable land due to the use of polluted water for irrigation. The polluted water stops the growth of plants. This has caused a greater damage to the environment. The pollution of water has threatened the people to a greater extent. The water after treatment using reverse osmosis were tested and analyzed. The physico-chemical parameters of water are within the permissible limit. Hence it is advised to the residents of Iron Industry to install a domestic reverse osmosis plant in order to convert the available ground water to potable waters. The water becomes suitable for drinking purpose with a low TDS of 40 mg $L^{-1}$. Reverse osmosis has been successfully applied on a large scale for the treatment of effluent and the polluted water.

In the present study the Iron Industry effluent are treated using RO plant and treatment can be recommended to all iron industries. The same reverse osmosis method can also be applied to other industry effluent.

## REFERENCES

[1]Cartwright, P.S. *Desalination*, **1985**, *56*, 17.

[2]Sinisgalli, P. and McNutt, J., *J. Am. Water Works Assoc.*, **1986**, 47.

[3]McCray, S., Wycherley, R., Newbold, D. and Ray, R., "A Review of Wastewater Treatment Using Membranes", *Int. Congr. Membranes Membrane Process*, **1990**, August 20-24, Chicago, Illinois.

[4]Cartwright, P. S., "Membranes for Industrial Wastewater Treatment - a Technical/Application Perspective", *Int. Congr. Membranes Membrane Process*, **1990**, August 20-24, Chicago, Illinois

[5]Cartwright, P. S., *Desalination*, **1991**, *83*, 225.

[6]Williams, M., Bhattacharyya, D., Ray, R., and McCray, S., "Selected Applications", in *Membrane Handbook*, W.S.W. Ho and K.K. Sirkar, ed., **1992,** pp. 312-354, Van Nostrand Reinhold, New York.

[7]Ranganathan K., Karunagaran K., Sharma D. C., *Resour. Conserv. Recycl.*, **2007**, *50*, 306–318.

[8]Ramesh Babu B., Parande A. K., Raghu S. and Prem Kumar T., J. Cotton Sci., **2007**, *11*, 141–153.

[9]Pandia Rajan A., Dheenadayalan M. S., *Res. J. Recent Sci.*, **2013**, 1-8.

[10]Slater, C., Ahlert, R. and Uchrin, C., *Desalination*, **1983a**, *48*, 171.

[11]Ghabris, A., Abdel-Jawad, M., and Aly, G., *Desalination*, **1989**, *75*, 213.

# SYNTHESIS, CHARACTERIZATION AND *IN VITRO* ANTICANCER ACTIVITY OF Co(II), Ni(II), Cu(II), AND Zn(II) COMPLEXES WITH 4-[{3-(4-BROMOPHENYL)-1-PHENYL-1H-PYRAZOL-4-YLMETHYLENE}-AMINO]-3-MERCAPTO-1,2,4-TRIAZIN-5-ONE

## Kiran Singh[a]*, Ritu Thakur[a] and Gaurav Kumar[b]

Schiff base derived from the condensation of 3-(p-bromophenyl)-1-phenyl-1H-pyrazolecarboxaldehyde with 4-amino-3-mercapto-1,2,4-triazin-5-one and its Co(II), Ni(II), Cu(II) and Zn(II) metal complexes have been synthesized in 1:1 and 1:2 molar ratios. Ligand and its metal complexes are characterized by various physicochemical techniques. On the basis of these techniques, octahedral geometry deduced for Co(II), Ni(II) and Zn(II) complexes and square planar for Cu(II) complexes. Low molar conductance values of all the metal complexes reveal their non-electrolytic nature. All the synthesized complexes have been screened *in vitro* for antibacterial activity against *S. aureus*, *B. subtilis*, *P. aeruginosa* and *E. coli* and antifungal activity against *C. albicans* and *S. cerevisiae*. It has been found that metal complexes show promising biological activity as compared to ligand. Schiff base and its metal complexes have been screened against human breast cancer cell lines by using the MTT [3-(4,5-dimethylthiazol-2-yl)-2,5-diphenyltetrazolium bromide] assay. *In vitro* anticancer cell lines results indicate that metal complexes exhibit significant activity on MCF-7.

* Corresponding Authors
    E-Mail: kiransinghkuk@yahoo.co.in
[a]  Department of Chemistry, Kurukshetra University, Kurukshetra 136119, Haryana, India
bDepartment of Biochemistry, Delhi University, Delhi 110021, India

## Introduction

Today, cancer is a major health problem around the globe. It increases at an alarming rate and cause about 13% of all the death.[1] To overcome this problem, it is necessary to develop the new potent anticancer agents. Now a days, Pt(II) based anticancer drugs have been used for clinical chemotherapy but they have severe side effects. Therefore, more interest has been drawn in the synthesis of less toxic non-platinum metal complexes.[2] Coordination complexes of heterocyclic moiety especially pyrazole based derivatives paid much attention in the recent years. Pyrazoles emerged as powerful scaffold in the field of organic synthesis as they have been extensively used to design pharmaceuticals and agrochemicals.[3,4] Further, existing literature indicates that pyrazole moiety possess unique position in medicinal chemistry as they exhibit wide range of bioactivities like anticancer,[5] anticonvulsant,[6] antidepressant,[7] antipyretic,[8] anti-inflammatory,[9] antiviral,[10] antihistaminic,[11] etc. Due to their diverse biological applications, this structural motif has been used as starting material for the formation of various Schiff bases and their corresponding metal complexes.[12] Pyrazole based biologically active ligands and their complexes with transition metals such as Co, Ni, Cu, Zn, Pd and V show broad range of biological activities as well as medicinal properties.[13-15] Therefore, all aforementioned applications paved the way towards the development of Schiff bases and their metal complexes as new chemotherapeutic agents. Hence, all these findings

prompted us to synthesize pyrazole based ligand and variety of metal complexes. Based on the above observations, present article focused on the synthesis of Co(II), Ni(II), Cu(II) and Zn(II) complexes with new Schiff base 4-[{3-(4-bromophenyl)-1-phenyl-1H-pyrazol-4-ylmethylene}-amino]-3-mercapto-1,2,4-triazin-5-one and screened them against human breast cancer cell lines.

## Experimental

Materials and Methods All the used chemicals and solvents were of analytical grade. ^{1}H-NMR spectra of the newly synthesized compounds were recorded on Bruker ACF 300 spectrometer at 300 MHz in $CDCl_3$/$d_6$-DMSO using 'TMS' as reference compound. IR spectra of the Schiff base and its metal complexes have been examined in KBr pellets/Nujol mulls on a MB-3000 ABB spectrometer. Electronic spectra of metal complexes were recorded on T 90 (PG Instruments ltd) UV/VIS spectrometer in DMF in the region 1100-200 nm. Magnetic moment measurements were carried out on Vibrating Sample Magnetometer at Institute Instrumentation Centre, IIT Roorkee. Fluorescence spectra of the ligand and metal complexes were recorded on SHIMADZU RF-5301 PC spectrophotometer. ESR spectra of Cu complexes were recorded under the magnetic field 3000 Gauss at frequency 9.1 GHz by using Varian E-112 ESR spectrometer at SAIF, IIT Bombay. Cyclic voltammetry measurements of Cu(II) complexes was recorded on Ivium Stat Electrochemical Analyzer with three electrode system of glassy carbon as the working electrode, a platinum wire as auxiliary electrode and Ag/AgCl as the reference electrode. Thermogravimetric analysis was obtained on a Perkin Elmer (Pyris Diamond) instrument at heating rate of 10°C Min⁻¹ by using alumina powder as reference.

Synthesis 4-amino-3-mercapto-1,2,4-triazin-5-one (AMOT) was synthesized according to reported procedure.[16]

**Synthesis of 4-[{3-(4-bromophenyl)-1-phenyl-1H-pyrazol-4-ylmethylene}-amino]-3-mercapto-1,2,4-triazin-5-one (HL).**

An ethanolic solution of AMOT (1.00 g, 6.94 mmol) was refluxed with an ethanolic solution of 3-(p-bromophenyl)-1-phenyl-1H-pyrazolecarboxaldehyde (2.27 g, 6.94 mmol) for 10 hours. The product formed was cooled to room temperature, filtered, washed with ethanol and recrystallized with same solvent and then dried (Fig. 1).
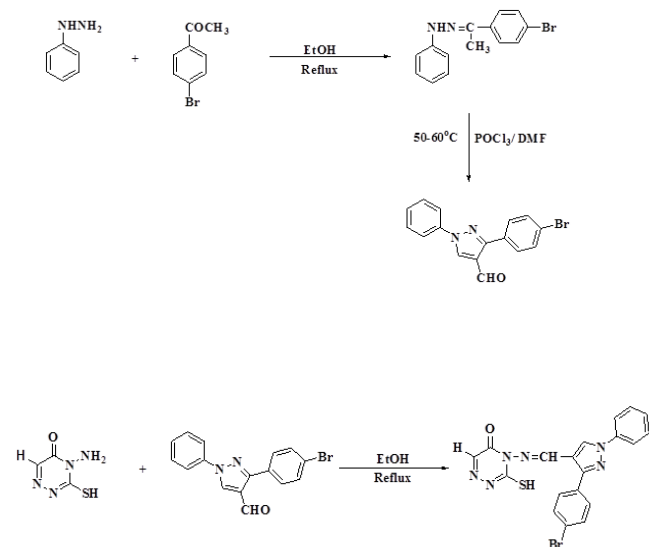


**Figure 1.** Synthesis of Schiff base

**Synthesis of 1:1 metal:ligand complexes**

Mixing the hot ethanolic solutions of Schiff base (0.20 g, 0.44 mmol) with hot ethanolic solutions of acetates of Co(II) (0.109 g, 0.44 mmol), Ni(II) (0.109 g, 0.44 mmol), Cu(II) (0.088 g, 0.44 mmol) and Zn(II) (0.096 g, 0.44 mmol). The colored product formed were immediately filtered, washed with warm water, aqueous ethanol, finally with acetone and then dried.

**Synthesis of 1:2 metal:ligand complexes**

Hot ethanolic solutions of metal acetates of Co(II) (0.109 g, 0.44 mmol), Ni(II) (0.109 g, 0.44 mmol), Cu(II) (0.088g, 0.44 mmol) and Zn(II) (0.096 g, 0.44 mmol) were treated with hot ethanolic solution of ligand (0.40 g, 0.88 mmol). The colored precipitates were formed immediately filtered, washed with warm water, aqueous ethanol and finally with acetone and then dried.

**Antimicrobial Assay**

The synthesized Schiff base and corresponding metal complexes were screened for antimicrobial activity against four bacterial strains (*Staphylococcus aureus* MTCC 96, *Bacillus subtilis* MTCC 121, *Pseudomonas aeruginosa* MTCC 741 and *Escherichia coli* MTCC 1652) and two fungal strains (*Candida albicans* MTCC 227 and *Saccharomyces cerevisiae* MTCC 170). All the bacterial cultures were procured from Microbial Type Culture Collection (MTCC), IMTECH, Chandigarh.

*In vitro* antimicrobial activity. Agar well-diffusion method was used to evaluate the newly synthesized Schiff base and its metal complexes. All the microbial culture were adjusted to 0.5 McFarland standard, which is visually comparable to a microbial suspension of approximately $1.5 \times 10^8$ cfu mL$^{-1}$. 20 ml of Muller Hinton agar medium was poured into each Petri plate and plates were swabbed with 100 µl inocula of the test microorganisms and kept for 15 minutes for adsorption using sterile cork borer of 8 mm diameter, wells were bored into the seeded agar plates and these were loaded with 100 µl volume (with concentration 4.0 mgml$^{-1}$) of each compound reconstituted in dimethyl sulphoxide (DMSO). All the plates were incubated at 37 °C for 24 hrs. Antimicrobial activity of each compound was evaluated by measuring the Zone of growth inhibition against the test organisms with zone reader (HiAntibiotic zone scale). DMSO was used as a negative control whereas Ciprofloxacin was used as positive control. This procedure was performed in three replicate plates for each organism.[17,18]

Minimum Inhibitory Concentration (MIC) MIC of the Schiff base and its metal complexes tested against bacterial stains through a modified agar well-diffusion method.[19] It is the lowest concentration of an antimicrobial compound that will inhibit the visible growth of a microorganism after overnight incubation.

**Anticancer Activity**

Anticancer activity was carried out in human breast cancer cell lines (MCF-7), obtained from National Center for Cell Science, Pune, India. The cells were cultured in Dulbecco's modified Eagles medium (DMEM) containing 10 % fetal bovine serum (FBS) at 37 °C in an atmosphere containing 5 % CO$_2$.

MTT assay MTT assay was performed on MCF-7 breast cancer cells to determine cell viability.[20] Briefly, $4 \times 10^3$ cells were seeded in 96 well plates. After incubation for 24 h at 37 °C under 5 % CO$_2$ in a humidified atmosphere, cells were exposed to different concentrations of cordycepin ranging from 0 to 100 µg mL$^{-1}$ for 48 h. MTT solution (10 µL, 5 mg mL$^{-1}$) was added to each well and further incubated for 4 h at 37 °C. The medium was removed and formazan crystals were dissolved by adding 100 µL of DMSO into each well and then shaking for another 20 min. Optical density (OD) was measured at 570 nm with a micro plate reader (Bio-Rad) and percentage of viability (φ) was calculated as follows:

$$\varphi = 100 \, \frac{OD_{test}}{OD_{control}}$$

Percent (%) cytotoxicity = 100 – (Percent viability)

**Table 1.** Physical characterization and analytical data of the ligand and metal complexes

| Compound | Color | MP (˚C) | Yield (%) | Found (Calcd) % | | | |
|---|---|---|---|---|---|---|---|
| | | | | C | H | N | M |
| HL [$C_{19}H_{13}N_6OSBr$] | Creamish yellow | 232-234 | 85 | 50.24 (50.34) | 2.60 (2.89) | 18.28 (18.54) | - |
| Co(L)(OAc).3H$_2$O [$C_{21}H_{21}BrCoN_6O_6S$] | Light green | 244-248 | 81 | 40.31 (40.40) | 3.28 (3.39) | 13.10 (13.46) | 9.25 (9.44) |
| Co(L)$_2$.2H$_2$O [$C_{38}H_{28}Br_2CoN_{12}O_4S_2$] | Light green | 250-254 | 79 | 45.58 (45.66) | 2.75 (2.82) | 16.70 (16.82) | 5.77 (5.90) |
| Ni(L)(OAc).3H$_2$O [$C_{21}H_{21}BrN_6NiO_6S$] | Light brown | 270-274 | 83 | 40.28 (40.41) | 3.28 (3.39) | 13.20 (13.47) | 9.26 (9.40) |
| Ni(L)$_2$.2H$_2$O [$C_{38}H_{28}Br_2N_{12}NiO_4S_2$] | Light brown | 264-268 | 77 | 45.46 (45.67) | 2.77 (2.82) | 16.73 (16.82) | 5.75 (5.87) |
| Cu(L)(OAc).H$_2$O [$C_{21}H_{17}BrCuN_6O_4S$] | Dark green | 256-260 | 82 | 42.48 (42.54) | 2.81 (2.89) | 14.02 (14.17) | 10.69 (10.72) |
| Cu(L)$_2$ [$C_{38}H_{24}Br_2CuN_{12}O_2S_2$] | Dark green | 276-280 | 80 | 47.01 (47.14) | 2.41 (2.50) | 17.22 (17.36) | 6.27 (6.36) |
| Zn(L)(OAc).3H$_2$O [$C_{21}H_{21}BrN_6O_6SZn$] | Light yellow | 280-282 | 78 | 39.90 (39.99) | 3.30 (3.36) | 13.25 (13.32) | 10.24 (10.37) |
| Zn(L)$_2$.2H$_2$O [$C_{38}H_{28}Br_2N_{12}O_4S_2Zn$] | Light yellow | 278-282 | 75 | 45.28 (45.37) | 2.70 (2.81) | 16.65 (16.71) | 6.43 (6.50) |

## Result and Discussion

Schiff base and its metal complexes are solid, colored, stable, non-hygroscopic in nature. All the metal complexes decomposed at high temperature on heating. They are insoluble in common organic solvent but soluble in DMF and DMSO. Their molar conductance values are low which consistent their non-electrolytic nature. The ligand and its metal complexes have been characterized with the help of IR, NMR, ESR, thermal, fluorescence, electron spectroscopic data, Magnetic moment measurements and cyclic voltammetry. Analytical data are presented in Table 1.

### Vibrational Spectra

IR analysis of Schiff base indicates the bidentate nature of the ligand (Table 2). Schiff base shows characteristic band at 1597 cm$^{-1}$ due to ν(-CH=N-) group. On complexation this band was shifted to lower frequency value it might be due to the formation of coordinate bond between azomethine N atom and metal ion.[21] A band appeared at 2793 cm$^{-1}$ ascribed to ν(-SH) which was not observed in the spectra of metal complexes shows the deprotonation of thiol group and bonding through S atom[22] which again confirmed by a new band appeared ~ 756 cm$^{-1}$ ascribed to ν (C-S). All the metal complexes show broad band located in the region 3271-3742 cm$^{-1}$ which is attributed to ν(-OH) stretching frequency of coordinated water molecules. In metal complexes, ν(M-N) band appears in the region 460-535 cm$^{-1}$ further confirms the chelation through N atom of azomethine group. Presence of ν(-OCOCH$_3$) group in 1:1 metal complexes highlighted by the band appeared in the region 1740-1744 cm$^{-1}$. The position of ν(-C=O) (at 1705 cm$^{-1}$) did not change on going from ligand to metal complexes implying the non-involvement of oxygen of keto group in coordination with metal ion.

## ¹H-Nuclear Magnetic Resonance Spectra

¹H-NMR spectra of Schiff base and its Zn(II) metal complexes have been recorded in DMSO-d$_6$ by using 'TMS' as internal standard and data are given in Table 3. ¹H-NMR spectrum of Schiff base shows the following signals; δ$_H$ (400 MHz, DMSO-d$_6$): 9.300 (1H, s, -CH=N-), 8.702 (1H, s, triazine-H), 7.907 (1H, s, pyrazole-H), 8.050 (2H, d, Ar-H), 7.580 (2H, t, Ar-H), 7.438 (1H, t, Ar-H), 7.787 (2H, d, Ar-H), 7.680 (2H, d, Ar-H), 13.90 (1H, br-s, -SH). The signal for azomethine proton deshielded in the spectra of Zn(II) complexes and appeared at δ 9.61 ppm indicates the complexation through azomethine nitrogen atom.[22] Signal of thiol group disappear in the spectra of Zn(II) complexes indicates the deprotonation of thiol group and complexation through S atom of thiol group.[23] Signals due to aromatic protons remain unaltered upon complexation. A new singlet observed at δ 4.009 ppm indicates the presence of coordinated water molecules in Zn(II) complexes. In 1:1 Zn(II) spectrum signal observed at δ 2.28 ppm due to methyl protons of –OCOCH$_3$ group.

### Electronic spectroscopy and magnetic moment measurements

To obtain the information regarding the stereochemistry of metal complexes, the electronic spectral analysis of 1:1 and 1:2 metal complexes have been carried out in 10$^{-3}$ mol L$^{-1}$ solution of DMF and summarized in table 4.

The absorption spectra of Co(II) complexes display two absorption bands in the region 10500-20161 cm$^{-1}$ and 10940-23108 cm$^{-1}$ which was reasonably assigned to $^4T_{1g}$ (F)→ $^4T_{2g}$ (F) (ν$_1$) and $^4T_{1g}$ (F)→ $^4T_{1g}$ (P) (ν$_3$) transitions respectively. The coordination field parameters (D$_q$, B, β, β %) have been calculated by using Band-Fitting equation. The values of Racah parameter (B) were found to be in the range 636-743 cm$^{-1}$ which is less than free ion value indicates overlapping of ligand metal orbitals.

**Table 2.** Characteristics IR frequencies (cm$^{-1}$) of Schiff base and its metal complexes

| Compound | $\nu_{(N=CH)}$ | $\nu_{(C-S)}$ | $\nu_{(S-H)}$ | $\nu_{(OCOCH3)}$ | $\nu_{(OH)}$ | $\nu_{(M-S)}$ | $\nu_{(M-N)}$ |
|---|---|---|---|---|---|---|---|
| HL | 1597 | - | 2777 | - | - | - | - |
| Co(L)(OAc).3H$_2$O | 1535 | 750 | - | 1744 | 3742 | 330 | 460 |
| Co(L)$_2$.2H$_2$O | 1535 | 756 | - | - | 3742 | 340 | 477 |
| Ni(L)(OAc).3H$_2$O | 1535 | 753 | - | 1740 | 3600 | 309 | 505 |
| Ni(L)$_2$.2H$_2$O | 1535 | 752 | - | - | 3742 | 333 | 496 |
| Cu(L)(OAc).H$_2$O | 1535 | 756 | - | 1744 | 3618 | 312 | 535 |
| Cu(L)$_2$ | 1535 | 754 | - | - | - | 350 | 489 |
| Zn(L)(OAc).3H$_2$O | 1535 | 757 | - | 1740 | 3271 | 365 | 481 |
| Zn(L)$_2$.2H$_2$O | 1535 | 758 | - | - | 3742 | 331 | 517 |

**Table 3.** $^1$H-NMR spectral data of Schiff base and Zn(II) complexes

| Compound | $^1$H-NMR (ppm) |
|---|---|
| HL [C$_{19}$H$_{13}$BrN$_6$OS] | 9.30 (s,1H, -CH=N-), 8.70 (s,1H, triazine-**H**), 7.90 (s, 1H, pyrazole-**H**), 8.05 (d, 2H, Ar-**H**), 7.58 (t, 2H, Ar-**H**), 7.43 (t, 1H, Ar-**H**), 7.79 (d, 2H, Ar-**H**), 7.68 (d, 2H, Ar-**H**), 13.90 (br-s, 1H, -SH) |
| Zn(L)(OAc).3H$_2$O [C$_{21}$H$_{21}$BrN$_6$O$_6$SZn] | 9.61 (s, 1H, -CH=N-), 8.67 (s, 1H, triazine-**H**), 7.89 (s, 1H, pyrazole-**H**), 8.02 (d, 2H, Ar-**H**), 7.56 (t, 2H, Ar-**H**), 7.42 (t, 1H, Ar-**H**), 7.78 (d, 2H, Ar-**H**), 7.66 (d, 2H, Ar-**H**), 2.28 (s, 3H, -OCOCH$_3$), 4.00 (s, 6H, -O**H**$_2$) |
| Zn(L)$_2$.2H$_2$O [C$_{38}$H$_{28}$Br$_2$N$_{12}$O$_4$S$_2$Zn] | 9.61 (s, 2H, -CH=N-), 8.67 (s, 2H, triazine-**H**), 7.89 (s, 2H, triazine-**H**), 8.02 (d, 4H, Ar-**H**), 7.56 (t, 4H, Ar-**H**), 7.41 (t, 2H, Ar-**H**), 7.78 (d, 4H, Ar-**H**), 7.67 (d, 4H, Ar-**H**), 4.00 (s, 4H, -O**H**$_2$) |

than one suggests the partial covalent character in the metal-ligand bond. In addition to this, the ratio of $\nu_2/\nu_1$ (1.71-1.73) indicates the octahedral geometry and observed magnetic moment values are found in the range of 3.2-3.4 BM which lies in the expected range of reported octahedral complexes.

A band observed in case of Cu(II) complexes in the region of 18510-19565 cm$^{-1}$ assigned to $^2B_{1g} \rightarrow {}^2A_{1g}$ indicates the square planar geometry of the copper complexes which is further confirmed by magnetic moment values 1.8-2.0 BM which is in the expected range of square planar complexes.
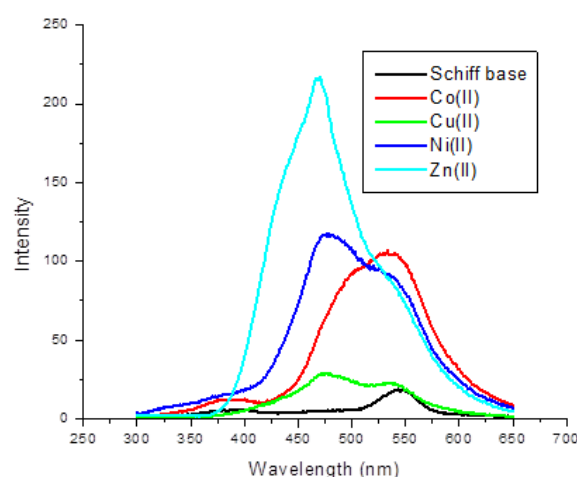


**Figure 2.** Fluorescence spectra of Schiff base and its metal complexes

**ESR Spectra**

ESR spectra of solid Cu(II) complexes were analyzed on X band at frequency 9.1 GHz under the magnetic field strength of 3000 G by using DPPH free radical as standard. The observed g values for Cu(L)OAc.H$_2$O ($g_\parallel$ = 2.12, $g\perp$ = 2.06, $g_{av}$ = 2.08, $G$ = 2.03) and for Cu(L)$_2$ ($g_\parallel$ = 2.13, $g\perp$ = 2.08, $g_{av}$ = 2.09, $G$ = 1.64). From experimental the $g_\parallel$ and $g\perp$ values are more than 2.04 suggest the axial geometry pattern for Cu(II) ion. The expression $g_\parallel > g\perp > 2.0023$ indicates that electron lies in d$_{x2-y2}$ orbital giving $^2B_{1g}$ as the ground state and suggest the square planar geometry for Cu(II) complexes.[26]

The nephelauxetic ratios (β) are found to be less than one suggests the partial covalent character in the metal-ligand bond. Magnetic moment value of Co(II) complexes are found in the range of 4.4-4.9 BM which is in the expected range (4.3-5.0) of octahedral complexes.[24]

The absorption spectra of Ni(II) complexes show three absorption bands in the range 9665-10600 cm$^{-1}$($\nu_1$), 16720-17621 cm$^{-1}$ ($\nu_2$) and 23818-24607 cm$^{-1}$ ($\nu_3$) assigned to $^3A_{2g}$ (F)$\rightarrow {}^3T_{2g}$ (F) ($\nu_1$), $^3A_{2g}$ (F)$\rightarrow {}^3T_{1g}$ (F) ($\nu_2$) and $^3A_{2g}$ (F)$\rightarrow {}^3T_{1g}$ (P) ($\nu_3$) transitions respectively. The coordination field parameters ($D_q$, $B$, β, β %) have also been calculated for Ni(II) complexes which are indicative of octahedral geometry.[25] The values of Racah parameter (B) were found to be in the range 759-769 cm$^{-1}$ which is less than free ion value (1041 cm$^{-1}$) indicates overlapping of ligand metal orbitals. The nephelauxetic ratios (β) are found to be less

**Table 4.** Electronic spectral data and ligand field parameters of metal complexes

| Compound | $\Lambda_{max}$ (cm$^{-1}$) | Band Assignment | $D_q$ (cm$^{-1}$) | $B$ (cm$^{-1}$) | $\nu_2/\nu_1$ | $\beta$ | $\beta$ % |
|---|---|---|---|---|---|---|---|
| Co(L)(OAc).3H$_2$O | 10500 | $^4T_{1g}$ (F) $\to$ $^4T_{2g}$ (F) ($\nu_1$) | 1039 | 636 | 1.99 | 0.655 | 34.5 |
|  | 20890* |  |  |  |  |  |  |
|  | 20161 | $^4T_{1g}$ (F) $\to$ $^4T_{1g}$ (P) ($\nu_3$) |  |  |  |  |  |
| Co(L)$_2$.2H$_2$O | 10940 | $^4T_{1g}$ (F) $\to$ $^4T_{2g}$ (F) ($\nu_1$) | 1216.8 | 743 | 2.11 | 0.765 | 23.5 |
|  | 23108* |  |  |  |  |  |  |
|  | 20865 | $^4T_{1g}$ (F) $\to$ $^4T_{1g}$ (P) ($\nu_3$) |  |  |  |  |  |
| Ni(L)(OAc).3H$_2$O | 9665 | $^3A_{2g}$ (F) $\to$ $^3T_{2g}$ (F) ($\nu_1$) | 966.5 | 769 | 1.73 | 0.739 | 26.1 |
|  | 16720 | $^3A_{2g}$ (F) $\to$ $^3T_{1g}$ (F) ($\nu_2$) |  |  |  |  |  |
|  | 23818 | $^3A_{2g}$ (F) $\to$ $^3T_{1g}$ (P) ($\nu_3$) |  |  |  |  |  |
| Ni(L)$_2$.2H$_2$O | 10281 | $^3A_{2g}$ (F) $\to$ $^3T_{2g}$ (F) ($\nu_1$) | 1028 | 759 | 1.71 | 0.729 | 27.1 |
|  | 17621 | $^3A_{2g}$ (F) $\to$ $^3T_{1g}$ (F) ($\nu_2$) |  |  |  |  |  |
|  | 24607 | $^3A_{2g}$ (F) $\to$ $^3T_{1g}$ (P) ($\nu_3$) |  |  |  |  |  |

The *G* (Axial symmetry parameter) value of the complex found to be less than 4.0 indicating the considerable exchange interaction in the Cu(II) centers.[27] The value of $g_{av}$ > 2.0023 (free electron) estimated from the expression:

$$g_{av} = 1/3 \ (g_{\parallel} + 2g_{\perp})$$

This is consistent with partial covalent property of Cu(II) complexes.

**Fluorescence Spectral Studies**

Fluorescent emission spectra of Schiff base and its 1:2 metal complexes have been recorded in DMF with 10$^{-3}$ molar concentration (Fig. 2). The fluorescent property of the ligand shows significant changes (enhancement in fluorescent intensity, shift of emission wavelength) when it is coordinated in metal and form complexes.[28] Fluorescence of Schiff base was quenched by the PET process due to presence of lone pair of electrons on N atom of Schiff base.[29] Metal ions are engaged with lone pair of electrons by formation of coordinate bonding, PET process is blocked and fluorescent intensity increases in metal complexes. Zn(II) metal complexes show more enhancement with emission wavelength of 470 nm whereas Co(II), Ni(II) and Cu(II) complexes show emission wavelength at 533 nm, 478 nm, and 535 nm respectively. A weak emission band observed at 543 nm for Schiff base. Enhancement order of fluorescence: Schiff base < Cu(II) < Co(II) < Ni(II) < Zn(II).

**Thermogravimetric Analysis**

Thermogravimetric analyses of Co(L)(OAc).3H$_2$O, Ni(L)$_2$.2H$_2$O, Cu(L)(OAc).H$_2$O and Zn(L)$_2$.2H$_2$O complexes have been carried out in temperature range of 50-700 °C in air atmosphere at heating rate of 10 °Cmin$^{-1}$ by using α-Al$_2$O$_3$ as reference. Different decompositions are represented in table 5 and Fig. 3. The Thermogravimetric curves are further supported by the DTA curves.

Decomposition of Co(L)(OAc).3H$_2$O took place in three steps. First decomposition step (100-220 °C) involved mass loss of 8.10 % (Calcd. 8.65 %) consistent with removal of three water molecules. Second decomposition step confined

to removal of organic and acetate moieties with mass loss 59.80 % (Calcd. 61.54 %) in the temperature range 221-510 °C. Third decomposition step has been observed in the range 511-570 °C with mass loss 19.50 % (Calcd. 20.35 %) corresponds to removal of triazine ring leaving CoO as residue.

Thermal study of Ni(L)$_2$.2H$_2$O has been carried out in three stages. First stage occurred between 95-210 °C with mass loss 3.00 % (Calcd. 3.60 %) assigned to removal of two water molecules. Second stage (211-450 °C) results in mass loss 63.75 % (Calcd. 65.07 %) corresponds to loss of organic moiety. Third stage (451-620 °C) involved mass loss of 23.00 % (Calcd. 25.43 %) assigned to removal of triazine ring leaving NiO as residue.
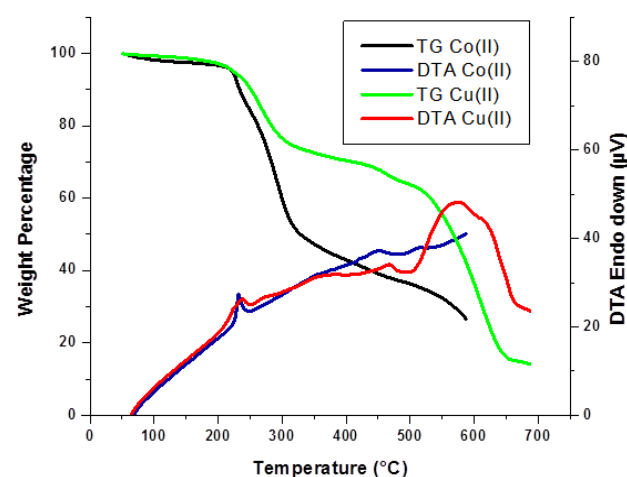


**Figure 3.** Thermogravimetric and DTA plot of a) Co(L)(OAc).3H$_2$O b) Cu(L)(OAc).H$_2$O

Thermal data of Cu(L)(OAc).H$_2$O suggest the copper complex is stable up to 90 °C. First degradation step exhibited mass loss 3.00 % (Calcd. 3.03 %) in temperature range 90-150 °C, associated with loss of one water molecule. In second step organic and acetate moieties were removed in temperature range 151-590 °C with mass loss 63.45 % (Calcd. 64.80 %). Third step (591-660 °C) associated with loss of triazine ring with mass loss 20.35 % (Calcd. 21.43 %) leaving CuO as residue.

**Table 5.** Thermogravimetric results of 1:1and 1:2 metal(II) complexes

| Compound | TG range (°C) | % Mass loss Found (Calcd.) | Decomposed moiety | Residue, % Found (calcd). | Residue |
|---|---|---|---|---|---|
| Co(L)(OAc).3H$_2$O [C$_{21}$H$_{21}$CoN$_6$O$_6$SBr] | 100-220 221-510 511-570 | 8.65 (8.10) 61.54 (59.80) 20.35 (19.50) | H$_2$O Organic & OAc moiety Triazine ring | 9.5 (12) | CoO |
| Ni(L)$_2$.2H$_2$O [C$_{38}$H$_{28}$N$_{12}$NiO$_4$S$_2$Br$_2$] | 95-210 211-450 451-620 | 3.00 (3.60) 63.75 (65.07) 23.00 (25.43) | H$_2$O Organic moiety Triazine ring | 6.50 (7.48) | NiO |
| Cu(L)(OAc).H$_2$O [C$_{21}$H$_{17}$CuN$_6$O$_4$SBr] | 90-150 151-590 591-660 | 3.03 (3.00) 64.80 (63.45) 21.43 (20.35) | H$_2$O Organic & OAc moiety Triazine ring | 10.74 (13.41) | CuO |
| Zn(L)$_2$.2H$_2$O [C$_{38}$H$_{28}$N$_{12}$O$_4$S$_2$Br$_2$Zn] | 110-230 231-350 351-600 | 2.85 (3.58) 62.75 (64.62) 23.50 (25.26) | H$_2$O Organic moiety Triazine ring | 7.00 (8.12) | ZnO |

The TG curve of Zn(L)$_2$.2H$_2$O shows three degradation steps. First degradation step has been observed with mass loss 2.85 % (Calcd. 3.58 %) from temperature range 110-230 °C corresponds to removal of two water molecules. Second degradation step (231-350 °C) assigned to removal of organic moiety with mass loss 62.75 % (Calcd. 64.62 %). Third mass loss 23.50 % (Calcd. 25.26 %) observed in temperature range 351-600 °C indicates the removal of triazine ring leaving ZnO as residue.

**Cyclic voltammogram**

The electrochemical feature of Cu(II) complexes was investigated in DMF solution by taking tetrabutylammoniumperchlorate as supporting electrolyte at room temperature. The repetitive scan were carried out at 100 mV s$^{-1}$ within potential range of 1.0 to -1.0 V. Forward scan of Voltammogram of Cu(L)(OAc).H$_2$O and Cu(L)$_2$ show reduction peaks at $E_{Pc}$ = 0.10 V and $E_{Pc}$ = 0.09 V respectively associated with Cu$^{2+/+}$ couple and reverse scan show oxidation peaks at $E_{Pa}$ = -0.90 V and $E_{Pa}$ = -0.65 V respectively associated with Cu$^{+/2+}$ couple. The peak separation data found to be $\Delta E_P$ = 0.8 V and 0.56 V. The analysis of cyclic voltammogram indicates the quasireversible one electron transfer process.[30,31]

**Biological Screening**

Biological screening of Schiff base and its metal complexes have been studied against standard microbial strains of *B. subtilis*, *S. aureus*, *E. coli*, *P. aeruginosa*, *C. albicans* and *S. cerevisiae* (Fig. 4). To find out the minimum concentration of ligand and its complexes which inhibit the visible growth of microbes, the compounds were tested for *invitro* biological evaluation. It was observed that ligand was biologically active but their metal complexes show more pronounced activity which can be rationalized by Overtone's concept[32] and Tweedy's chelation theory.[33] According to Overtone's concept of cell permeability, the lipid membrane surrounding the cell favors the passage of only lipid-soluble material; therefore, liposolubility is a crucial factor which controls the antimicrobial activity.

Tweedy suggest that chelation could facilitate the passage of complexes across the cell membrane. On chelation polarity of metal ion reduces because of partial sharing of its positive charge with donor groups and increase in the delocalization of π-electrons over the whole chelate ring. Among the complexes, Co(L)(OAc).3H$_2$O, Co(L)$_2$.2H$_2$O and Cu(L)(OAc).H$_2$O were highly active against gram positive bacteria with diameter of inhibition zone ranging between 20-22 mm, 19-23 mm and 17-23 mm respectively. Cu(L)(OAc).H$_2$O and Cu(L)$_2$ show high activity against gram negative bacteria with inhibition zone ranging between 19-23 mm and 20-22 mm respectively. Compounds Co(L)$_2$.2H$_2$O, Zn(L)(OAc).3H$_2$O and Zn(L)$_2$.2H$_2$O were very effective against yeast with inhibition zone between 13-17 mm, 14-20 mm and 13-23 mm respectively.
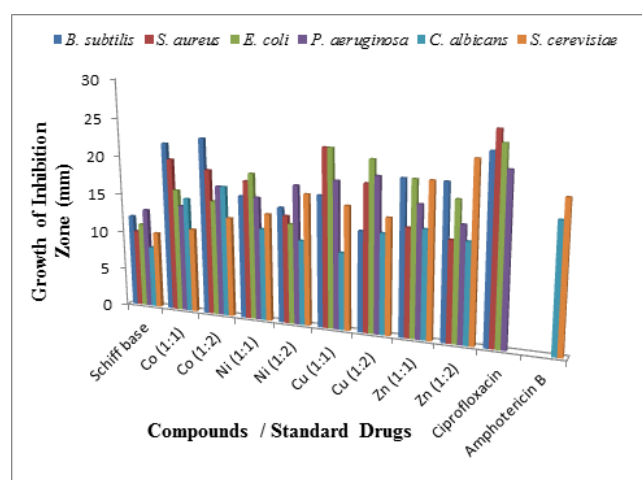


**Figure 4.** Biological activity of Schiff base and metal complexes with standard drugs

The compounds which shows highest diameter of growth of inhibition zone were selected to test their MIC values. Compounds Co(L)(OAc).3H$_2$O, Co(L)$_2$.2H$_2$O and Cu(L)(OAc).H$_2$O shows lowest MIC value 12.5 µg mL$^{-1}$ against gram positive bacteria and compounds Co(L)(OAc).3H$_2$O and Co(L)$_2$.2H$_2$O shows lowest MIC value 12.5 µg mL$^{-1}$ against *C. albicans*.
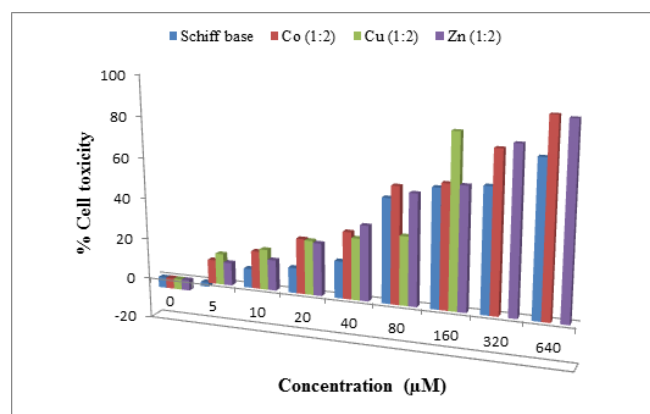
**Figure 5.** Effect of concentration of Schiff base and its metal complexes on % cytotoxicity of human breast cancer cell line

**Anticancer activity**

In order to check the cytotoxicity of complexes, Schiff base and its metal complexes has been evaluated against human breast cancer cell lines (MCF-7) within 5-640 µM concentration range (Fig. 5). Doxorubicin was taken as reference compound. The $IC_{50}$ value obtained from *in vitro* evaluation demonstrate the significant cytotoxicity of the tested metal complexes against MCF-7 cell lines (Fig. 6). Metal complexes are found to be more cytotoxic ($IC_{50}$ = 98.66-106.90 µM) against MCF-7 cell lines as compared to Schiff base. Compound 4 i.e. Zn (1:2) complex shows highest cytotoxicity with $IC_{50}$ value 98.66 µM followed by Co (1:2) complex with $IC_{50}$ value 100.04 µM and then Cu (1:2) complex with $IC_{50}$ value 106.90 µM. In this series, metal complexes were found to be most active as compared to Schiff base and their descending order are Zn(II) > Co(II) > Cu(II) > Schiff base.
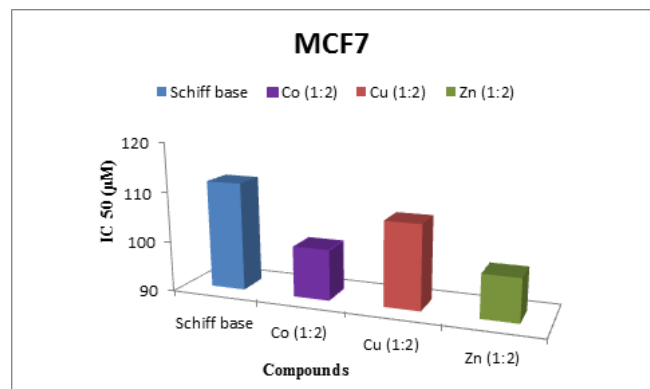


**Figure 6.** Comparative $IC_{50}$ value of Schiff base and its metal complexes against MCF-7 cell lines

This enhancement of anticancer activity in metal complexes may be due to coordination.[34] Pyrazoles is a prevalence scaffold in the synthesis of anticancer active compounds and their efficiency increases when they coordinated with metal ion. Structure activity relationship (SAR) study of complexes reveals that coordination via azomethine N atom and S atom enhances the anticancer activity.

**Stastical Analysis**

By using SPSS Stastical software (version 16), level of significance was analyzed through one way ANOVA followed by Duncan test. It was observed that $^*P < 0.05$ and $^{**}P < 0.01$, ns = non-significant. All the values were expressed as mean ± standard error of mean (SEM) with % cytotoxicity.

**Conclusions**

By combining the information coming from different conventional techniques, octahedral geometry has been deduced for Co(II), Ni(II), Zn(II) complexes and square planar for Cu(II) complexes (Fig. 7). Antimicrobial screening indicates that metal complexes are more active as compared to Schiff base. Specially, Co(II) and Zn(II) complexes have shown more activity. *In vitro* anticancer cell lines activity reveals that metal complexes show moderate anticancer activity over Schiff base. Among them Zn(II) complex found to be more efficient against MCF-7 cell lines. It is concluded that metal complexes can be used as lead molecule for new anticancer agents.

**Supplementary Information**

All the information pertaining to characterization of Schiff base and its metal complexes using ^{1}H-NMR (Fig. S1, S2, S3), ESR spectra (Fig. S4) and thermogravimetric plot (Fig. S5), Biological data (tables S1, S2) and Stastical data of tested compounds (S3) are given in the supporting information.

**Acknowledgements**

**References**

[1]Ahsan, M. J., Khalilullah, H., Yasmin, S., Jadav, S. S., Govindasamy, *J. Biomed. Res. Int.,* **2013,** 1.

[2]Huang, Y., Wang, W. X., Zhou, X. J., *Indian J. Chem.,* **2014**, *53A*, 793.

[3]Beheshti, A., Lalegani, A., Noshadian, A., Bruno, G., Rubdari, H. A., *Polyhedron,* **2015**, *85*, 690.

[4]Damljanovic, I., Vukicevic, M., Radulovic, N., Palic, R., Ellmerer, E., Ratkovic, Z., Joksovic, M. D., Vukicevic, R. D., *Bioorg. Med. Chem. Lett.,* **2009**, *19*, 1093.

[5]Sakai, K., Tomista, Y., Ue, T., Goshima, K., Ohminato, M., Tsubomora, T., Matsumoto, K., Ohmura, K., Kawakami, K., *Inorg. Chim. Acta,* **2000**, *297*, 64.

[6]Malecki, J. G., Palion, J., Oboz, M., Grori, T., *Polyhedron,* **2014**, *73*, 81.

[7]Saha, N. C., Mandal, S., Das, M., Khatun, N., Mitra, D., Samanta, A., Slawin, A. M. Z., Butcher, R. J., Saha, R., *Polyhedron*, **2014**, *68*, 122.

[8]Konar, S., Jana, A., Das, K., Ray, S., Chatterjee, S., Kar, S. K., *Inorg. Chim. Acta*, **2013**, *395*, 1.

[9]Wei, J., Zhang, D., Yang, Q., Chen, S., Gao, S., *Inorg. Chem. Commun.*, **2013**, *30*, 13.

[10]Kumar, H., Saini, D., Jain, S., Jain, N., *Eur. J. Med. Chem.,* **2013**, *70*, 248.

[11]Casas, J. S., Castellano, E. E., Ellena, J., Garcia-Tasende, M. S., Perez-Paralle, M. L., Sanchez, A., Sanchez-Gonzalez, A., Sordo, J., Touceda, A., *J. Inorg. Biochem.,* **2008**, *102*, 33.

[12]El-Sawy, E. R., Ebaid, M. S., Abo-Salem, H. M., Al-Sehemi, A. G., Mandour, A. H., *Arab. J. Chem.,* **2014**, *7*, 914.

[13]Siddiqui, N., Andalip, Bawa, S., Ali, R., Afzal, O., Akhtar, M. J., Azad, B., Kumar, R., *J. Pharm. Bioallied Sci.,* **2011,** *3*, 194.

[14]Hanumanagoud, H., Basavaraja, K. M., *Der Pharm. Chem.,* **2013**, *5*, 87.

[15]Kulkarni, N. V., Kamath, A., Budagumpi, S., Revankar, V. K., *J. Mol. Struct.,* **2011**, *1006*, 580.

[16]Ramasubramanian, A. S., Bhat, B. R., Dileep, R., *Rasayan J. Chem.,* **2010**, *3*, 122.

[17]Ahmad, I., Beg, A. Z., *J. Ethnopharmacol.,* **2001,** *74*, 113.

[18]Andrews, J. M., *J. Antimicrob. Chemother.,* **2011**, *48*, 5.

[19]Aneja, K. R., Sharma, C., Joshi, R., *J. Microbiol.,* **2011,** *4,* 175.

[20]Anjomshoa, M., Hadadzadeh, H., Torkzadeh-Mahani, M., Fatemi, S. J., Abeli-Sardou, M., Rudbari, H. A., Nardo, V. M., *Eur. J. Med. Chem.,* **2015**, *96*, 66.

[21]El-Metwally, N. M., Gabr, I. M., Shallaby, A. M., *J. Coord. Chem.,* **2005**, *58*, 1145.

[22]Singh, K., Kumar, Y., Puri, P., Sharma, C., Aneja, K.R., *Med. Chem. Res.,* **2012**, *21*, 1708.

[23]Raman, N., Sobha, S., Mitu, L., *J. Saudi Chem. Soc.,* **2013**, *17*, 151.

[24]Singh, K., Barwa, M. S., Tyagi, P., *Eur. J. Med. Chem.,* **2006**, *41*, 147.

[25]Chandra, S., Gupta, K., *Indian J. Chem.,* **2001**, *40A*, 775.

[26]Kivelson, D., Neiman, R., *J. Chem. Phy.,* **1961**, *35*, 149.

[27]Raman, N., Joseph, J., *J. Coord. Chem.,* **2009**, *62,* 1162.

[28]Kavitha, P., Reddy, K. L., *Bioinorg. Chem. Appl.,* **2014**, 1.

[29]Basak, S., Sen, S., Banerjee, S., Mitra, S., Rosair, G., Rodriquez, M. T. G., *Polyhedron,* **2007**, *26*, 5104.

[30]Gokmese, E., *Int. J. Electrochem. Sci.,* **2011**, *6,* 103.

[31]Franco, E., Torres, E. L., Mendiola, M. A., Sevilla, M. T., *Polyhedron,* **2000**, *19*, 441.

[32]Break, M. K., Tahir, M. I. M., Crouse, K. A., Khoo, T. J., *Bioinorg. Chem. Appl.,* **2013,** 1.

[33]Chohan, Z. H., Supran, C. T., Scozzafava, A., *J. Enzyme Inhib. Med. Chem.,* **2004**, *19*, 79.

[34]El-Tabl, A. S., El-Waheed, M. M. A., Wahba, M. A., El-Fadl, N. A. E. H. A., *Bioinorg. Chem. Appl.,* **2015** doi: 10.1155/2015/126023.

# SYNTHESIS, STRUCTURE AND MAGNETIC PROPERTIES OF A COPPER(II) COMPLEX OF 5-NITRO-2-HYDROXYPYRIDINE AND PYRAZINE: [Cu(5-NO$_2$-2-HOPy)(Pz)$_2$(H$_2$O)](ClO$_4$)$_2$·H$_2$O

## M.C. Monk[a], C. P. Landee[b], M. M. Turnbull[a] and J. L. Wikaira[c]

The synthesis, structure, and magnetic properties of [Cu(5-NO$_2$-2-HOPy)(pz)$_2$(H$_2$O)] (ClO$_4$)$_2$·H$_2$O (pz = pyrazine) (**1**) are reported. Crystals were characterized using IR, combustion analysis, X-ray powder diffraction, single crystal X-ray diffraction, and temperature-dependent magnetic susceptibility measurements. Compound **1** crystallizes in the monoclinic space group P2$_1$/c. The crystal structure consists of copper/pyrazine chains parallel to the *c*-axis with terminal pyrazine groups found perpendicular to the bridging pyrazine molecules creating a zig-zag chain structure. The 1D-system exhibits weak antiferromagnetic interactions of *J* = -7.58 K with no measurable interchain interactions.

[a]  Carlson School of Chemistry and Biochemistry, Clark University, 950 Main Street, Worcester, Massachusetts 01610
[b]  Department of Physics, Clark University, 950 Main Street, Worcester, Massachusetts 01610
[c]  Department of Chemistry, University of Canterbury, Private Bag 4800, Christchurch, New Zealand

## Introduction

Studies using coordination complexes have allowed for better understanding of the effects of local geometry, bond lengths and angles, and close interactions on the magnetic exchange pathways in a crystalline lattice.[1] The magnetic susceptibility of a crystalline lattice is dependent on the interaction between moments belonging to each metal ion's nearest neighbors and their corresponding spin values and may be affected by next-nearest neighbor interactions and on into the extended lattice. Overlapping electron wave functions may result in a decrease in the overall energy of the system and as a result, the exchange can then be understood with respect to the nature of the symmetric or asymmetric wave functions.[2] We, as a research group, seek to understand the changes in magnetic exchange that result from differing interconnectivity within a lattice.

Coordination complexes containing pyrazine as the ligand exhibit a wide range of magnetic exchange values from -2 to -46 K.[3-6] In studying one-dimensional quantum Heisenberg antiferromagnets, the d$^9$ configuration of the copper (II) ion has proven to be beneficial with a single unpaired electron creating a spin of ½ with nearly isotropic exchange. Copper's quenched orbital angular momentum as well as a g-value[7] near 2 suggests a negligible preference for alignment of the magnetic moment along a particular crystallographic axis. The effects of substituted pyrazines on the magnetic exchange within the coordination complexes have been observed,[8-10] but the effects of changing the electron density donated to a copper(II) through an additional ligand has not been studied systematically. The complex [Cu(C$_5$H$_4$ClNO)$_2$(C$_4$H$_4$N$_2$)(H$_2$O)$_2$](ClO$_4$)$_2$ is of great interest with its copper (II) ion, pyrazine bridges and pyridine groups with the potential to vary their electron donating or withdrawing character by changing the substituents on the pyridine ring.[11] This complex was

synthesized and structurally characterized, but the magnetic properties were not studied. The structure of the complex is shown in Figure 1. The 2-pyridone molecules function as terminal units exhibiting strong ligating ability[12] while pyrazine has weaker ligating ability, but the two nitrogen atoms allow pyrazine to act as a bridging bidentate ligand and create an efficient pathway for spin exchange and subsequent magnetic interactions.[13,14]



**Figure 1.** Molecular unit of [Cu(C$_5$H$_4$ClNO)$_2$ (C$_4$H$_4$N$_2$)(H$_2$O)$_2$] (ClO$_4$)$_2$

The azaphilic copper ion is expected to interact with both nitrogen atoms on the pyrazine molecule and together function as the repeating unit. In an attempt to understand the effect of electron density on magnetic exchange, a family of complexes with a similar molecular composition to the above complex is being prepared. The pyridone rings on the coordination complex allow for a single parameter, the electron density at the Cu(II) ion, to be tested without steric bulk interference. Addition of substituents on the 4, 5 and 6 positions on the pyridone ring will not affect spatial crowding near the copper ion resulting from the positions being planar and distant from the copper whereas substitutions on the pyrazine ring would greatly affect the geometry and binding at the copper. In the process of preparing additional members of this family, we have

observed serendipitous formation of a related product containing both bridging and terminal pyrazine molecules. We report here the synthesis, structure and magnetic properties of [Cu($C_5H_4N_2O_3$)($C_4H_4N_2$)$_2$($H_2O$)](ClO$_4$)$_2$·$H_2O$, **1**.

# EXPERIMENTAL

Copper (II) perchlorate hexahydrate, pyrazine and 2-hydroxy-5-nitro-pyridine (5-nitro-2-pyridone) were purchased from Sigma Aldrich. Materials were used as received without further purification. IR spectra were recorded via ATR on a Perkin-Elmer Spectrum 100 spectrometer. X-Ray powder diffraction was carried out on a Bruker AXS-D8 X-ray Powder Diffractometer. Elemental analysis was carried out by Marine Science Institute, University of California, Santa Barbara, CA 93106.

**Synthesis of aquapyrazine(2-hydroxy-5-nitropyridine)-copper(II) perchlorate hydrate,**
**[Cu($C_5H_4N_2O_3$)($C_4H_4N_2$)$_2$($H_2O$)](ClO$_4$)$_2$·$H_2O$ (1)**

Compound **1** was made as a byproduct in the attempted synthesis of [Cu($C_5H_4N_2O_3$)$_2$($C_4H_4N_2$)($H_2O$)$_2$] ( ClO$_4$)$_2$. Attempts to reproduce the synthesis of **1** have been unsuccessful to date. A solution of 2-hydroxy-5-nitro-pyridine (0.140g, 1.0 mmol) dissolved in 9.0 mL of a 50% methanol/ water solution with warming, was added to a solution of copper (II) perchlorate (0.369g, 1.0 mmol) dissolved in 2.0 mL of the same solvent. A methanol/water solution (3.0mL) of pyrazine (0.164g, 2.0 mmol) was then added. Colorless rod-like crystals separated from the solution after a few days and were isolated and confirmed to be recrystallized 2-hydroxy-5-nitro-pyridine through IR. Large dark blue crystals separated from the remaining solution after eleven days of slow evaporation. The colorless product was isolated in 6.2% yield (0.042 g) and dark blue product was isolated in 17.5% yield (0.118 g). The dark blue product proved to be **1**. IR (v in cm$^{-1}$): 1651 (m), 1611 (m), 1563 (w), 1507 (m), 1425 (m), 1358 (m), 1242 (w), 1216 (w), 1122(m), 1062 (s), 844 (m), 817 (m), 761 (w), 711 (w), 653 (m), 622 (s). CHN for $C_{13}H_{16}N_6O_{13}Cl_2Cu$, found (calculated): C: 26.6 (26.2), H: 2.52 (2.21), N: 13.7 (13.1).

**X-Ray Structure Analysis**

Data collection was carried out for **1** on an Agilent Technologies Gemini Eos CCX-ray diffractometer utilizing CuKα radiation (λ=1.5418 Å) with co-scans at 120.01(10) K employing a mirror monochromator. CrysAlisPro software was used to refine cell parameters while SCALE3 ABSPACK scaling algorithm was used for absorption corrections.[15] The structure was solved and refined using the SHELX97-2 program and a least squares analysis.[16] Non-hydrogen atoms were refined using anisotropic thermal parameters. Hydrogen atoms bonded to nitrogen or oxygen atoms were located in the difference Fourier maps and their positions refined using fixed isotropic thermal parameters.

The remaining hydrogen atoms were placed in geometrically calculated positions and refined using fixed isotropic thermal parameters. Crystallographic information and details of the data collection can be found in Table 1.

**Magnetic Susceptibility Data Collection**

Magnetic susceptibility data for **1** were collected using a Quantum Design MPMS-XL SQUID magnetometer. A weighed sample of the finely ground crystals was packed into a gelatin capsule. Data was collected on the measured moment using magnetic fields from 0 to 50 kOe at 1.8 K and several data points were collected as the field returned to 0 kOe to check for hysteresis effects; none were observed. Magnetization was then measured from 1.8 to 310 K in a 1 kOe field. The data collected were corrected for the background signal of the gelatin capsule and the sample mount. The data were also corrected for diamagnetic contributions of the constituent atoms, estimated via Pascal's constants,[6] and the temperature independent paramagnetism of the copper (II) ion. All data was fit using the Hamiltonian $H = -J\sum S_1 \cdot S_2$. The composition of **1** was analyzed by powder X-ray diffraction and compared to the single crystal structure prior to data collection. No impurities were observed.

**Table 1. X-ray data of compound 1.**

| Empirical formula | $C_{13}H_{16}Cl_2CuN_6O_{13}$ |
|---|---|
| Formula weight | 598.76 |
| Temperature | 120.01(10) K |
| Wavelength | 1.54184 Å |
| Space group | P2$_1$/c |
| *a* | 17.0258(2) Å |
| *b* | 12.15341(16) Å |
| *c* | 10.19594(13) Å |
| α | 90° |
| β | 92.0607(11)° |
| γ | 90° |
| Volume | 2108.39(5) Å$^3$ |
| Z | 4 |
| Density (calculated) | 1.886 Mg m$^{-3}$ |
| Absorption coefficient | 4.576 mm$^{-1}$ |
| *F*(000) | 1212 |
| Crystal size | 0.380 x 0.350 x 0.024 mm$^3$ |
| θ range for data collection | 4.47 to 76.78°. |
| Index ranges | -12 ≤ *h* ≤ 21, -15 ≤ *k* ≤ 15, -12 ≤ *l* ≤ 12 |
| Reflections collected | 15178 |
| Independent reflections | 4401 [*R*(int) = 0.0274] |
| Absorption correction | Semi-empirical from equivalents |
| Max. and min. transmission | 1.00000 and 0.56697 |
| Refinement method | Full-matrix least-squares on F$^2$ |
| Data / restraints / parameters | 4401 / 0 / 332 |
| Goodness-of-fit on *F*$^2$ | 1.054 |
| Final *R* indices [*I*>2σ(I)] | $R^1$ = 0.0362, $wR_2$ = 0.0934 |
| *R* indices (all data) | $R^1$ = 0.0374, $wR_2$ = 0.0944 |
| Extinction coefficient | 0.00330(16) |
| Largest diff. peak and hole | 1.485 near O6 and -0.649 e.Å- |

**Synthesis**

The reaction of copper perchlorate hexahydrate, pyrazine and 2-hydroxy-5-nitro-pyridine over heat in 50 % methanol and water formed a pale green solution. Cooling this solution and slow evaporation deposited **1** (Scheme 1). Starting material 2-hydroxy-5-nitro-pyridine is present in solution in lactam form (Scheme 2) and coordinated to the copper ion through the oxygen. Tautomeric equilibria of hydroxypyridines and corresponding pyridines are well studied.[17-19]

$$Cu(ClO_4)_2 \cdot 6H_2O + 2\,pz +$$

[Cu(C$_5$H$_4$N$_2$O$_3$)(pz)$_2$(H$_2$O)](ClO$_4$)$_2$ · H$_2$O
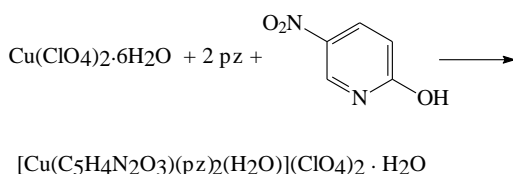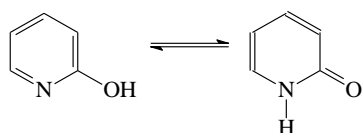
**Scheme 1**                    **1**

**Scheme 2**

**Crystal Structure Analysis**

Compound **1** crystallizes in the monoclinic space group P 2$_1$/*c*. The asymmetric unit is shown in Figure 2. Selected bond lengths and angles are given in Table 2. The atoms of the pyrazine and pyridone ring are numbered with consecutive addition of 10 (N1, N11, N21) for ease of discussion.
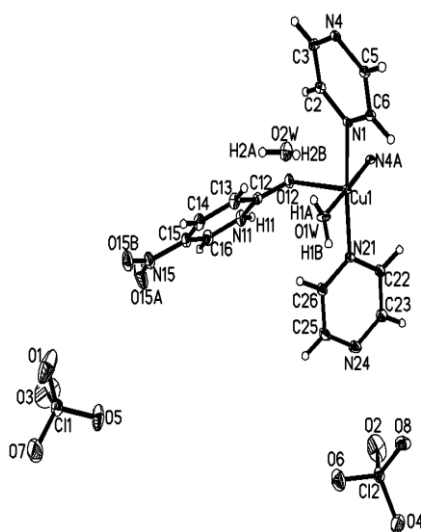
The Addison parameter ($\tau$) of 0.08 indicates that the Cu(II) ion has a nearly square pyramidal geometry[20] with each Cu(II) ion coordinated to one molecule of water, one 5-nitro-2-pyridone through the oxygen, two bridging pyrazines (parallel to the *c*-axis) and a terminal pyrazine. The copper ion sits on a general position. Cu1 is bonded to a molecule of 5-nitro-2-pyridone which occupies the axial position of the square pyramid as indicated by its maximum angle of 96.57(6)° to the other ligands.

2-Hydroxy-5-nitro-pyridine equilibrates to 5-nitro-2-pyridone in solution where the oxygen atom is coordinated to the copper ion. The pyridone ring is nearly planar as indicated by a maximum torsional angle of 0.8° (C13-C14-C15-C16) and the nitro group is nearly co-planar to the pyridone ring ($\angle$C14-C15-N15-O15B =2.2°) as would be expected due to conjugation.[21,22] The nitro group itself is planar as indicated by the summation of the angles around N15 (360.0°). The bound water molecule is planar as indicated by the angle summation, however, the H1A-O1W-H1B angle has expanded to 112(3)° suggesting that the water molecule is progressing toward a trigonal planar geometry rather than tetrahedral. This can be understood by the potential of a partial double bond character between O1W and Cu1 creating significant sp$^2$ character and increased π-donation to the copper ion further contributing to the change in electron density.

The pyrazine rings are nearly planar, as expected,[23] and exhibit maximum torsional angles within the rings of 1.2° for the bridging pyrazine ($\angle$C2-C3-N4-C5) and -1.1° for the terminal pyrazine ($\angle$C23-N24-C25-C26). The mean plane of the bridging pyrazine ring is canted 72.2° in relation to the mean plane of the terminal pyrazine ring while the symmetry equivalent bridging pyrazine ring is canted 81.6° with respect to the terminal pyrazine. The bridging pyrazine rings are nearly perpendicular with an angle of 85.3° between their mean planes resulting in a zig-zag chain structure.

**Figure 2.** Thermal ellipsoid plot of the asymmetric unit showing 50% probability ellipsoids. Only those H-atoms whose positions were refined are labeled. Symmetry operation for N4A (x,-y+3/2, z-1/2)

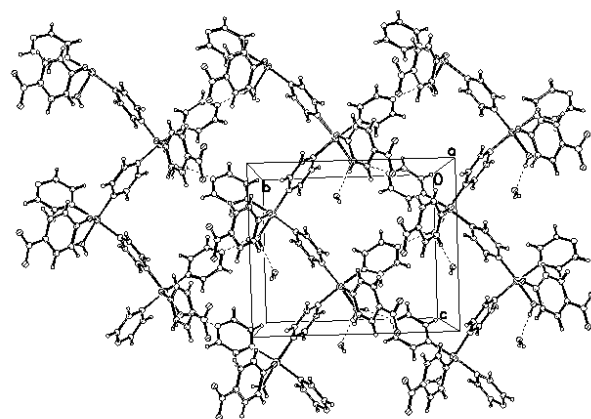**Figure 3.** Layer formed by bridging and terminal pyrazines parallel to the *bc* face of the lattice. Perchlorate and water molecules are in the interstitial space and actively stabilizing the lattice structure through hydrogen bonding. Dashed lines represent the hydrogen bonding between the hydrogen atoms on the water molecule to the coordinated water molecule as well as to nitrogen atoms on the terminal pyrazine.

**Table 2.** Selected bond lengths [Å] and angles [°] for **1**

| Bond | Distance | Bond | Angle |
|------|----------|------|-------|
| Cu1-O1W | 1.9523(16) | O1W-Cu1-N21 | 90.00(7) |
| Cu1-N21 | 2.0245(18) | O1W-Cu1-N4#1 | 176.61(7) |
| Cu1-N4#1 | 2.0391(17) | N21-Cu1-N4#1 | 92.97(7) |
| Cu1-N1 | 2.0463(17) | O1W-Cu1-N1 | 84.34(7) |
| Cu1-O12 | 2.2382(15) | N21-Cu1-N1 | 171.11(7) |
| | | N4#1-Cu1-N1 | 92.51(7) |
| | | O1W-Cu1-O12 | 90.65(6) |
| | | N21-Cu1-O12 | 90.33(7) |
| | | N4#1-Cu1-O12 | 90.96(6) |
| | | N1-Cu1-O12 | 96.57(6) |
| | | O15A-N15-O15B | 123.4(2) |
| | | O15A-N15-C15 | 118.8(2) |
| | | O15B-N15-C15 | 117.8(2) |
| | | Cu1-O1W-H1A | 123(2) |
| | | Cu1-O1W-H1B | 123(2) |
| | | H1A-O1W-H1B | 112(3) |

Symmetry transformations used to generate equivalent atoms: #1 x,-y+3/2,z-1/2   #2 x,-y+3/2,z+1/2

Compounds containing a zig-zag structure with bridging and terminal pyrazine molecules are unusual, but not unique. Previous reports include $Cu(pz)_2(CF_3SO_3)$,[24] $[\{Zn^tBu_2\}_3\{C_4H_4N_2\}_4]$[25] and $[Cu(HF_2)(pz)_2]SbF_6$.[6]

The –Cu-pz-Cu- chains are connected into layers parallel to the *bc* face of the crystal (Fig. 3) by hydrogen bonding networks between the oxygen atoms in the perchlorate ions to amine hydrogen atoms on the pyridone ring where the oxygen from the perchlorate ion serves as the acceptor. Hydrogen bonding is also observed between the free water molecules and N24 on the terminal pyrazine rings. The molecules contributing to hydrogen bonding within the lattice are shown in Figure 4. Hydrogen bond parameters are given in Table 3. The perchlorate ions and water molecules can be found occupying the interstitial spaces between bridging pyrazine chains. Compound **1** packs in pleated sheets parallel to the *bc*-face, exhibiting an aabb packing pattern (Fig. 5) where "a" is the pyridone rings and "b" is the copper-pyrazine layer. In looking at the packing of four single chains, adjacent complementary pairs of chains are offset from one another by ½ unit cell parallel to the *b*-axis rather than repeating in the same spatial orientation resulting in the aabb pattern.
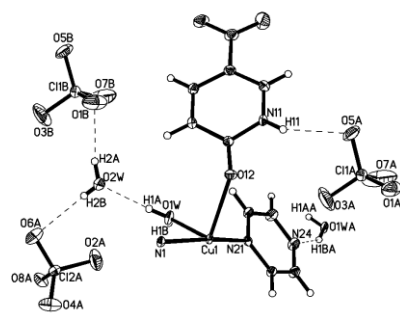


**Figure 4.** Thermal ellipsoid plot of 1 showing the symmetrically generated molecules of perchlorate ions and water molecules that play a role in hydrogen bonding.
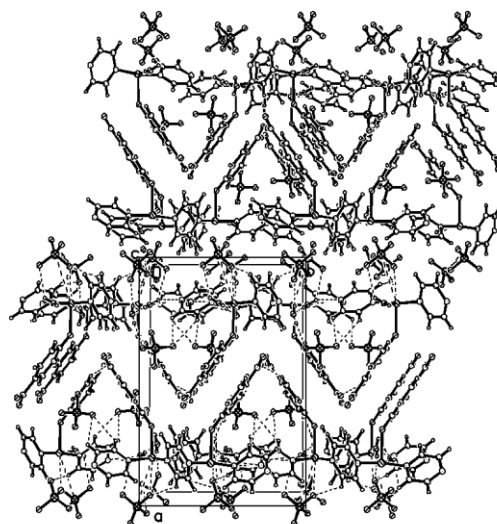


**Figure 5.** Packing structure of the layers viewed parallel to the *b*-axis and down the chains that run parallel to the *c*-axis.

The copper ions within a sheet are separated by a distance greater than 11.8 Å while the copper molecules between two sheets are separated by a distance greater than 8.0 Å.

**Magnetic Study**

Susceptibility data for **1** was collected in a 0.1 T field from 1.8 K to 310 K. The susceptibility of **1** shows rounded maxima near 5 K characteristic of low-dimensional antiferromagnetic behavior.[26] The low temperature of the maximum suggests weak interactions between Cu(II) ions. The data were fit to the S=1/2 Heisenberg linear chain model both with, and without, a Curie-Weiss (CW) correction for interchain interactions[2] and resulted in a $J$ = -7.49(2) K, Curie Constant ($C$) = 0.436(1) emu(K) mol(Oe)$^{-1}$ and a paramagnetic impurity ($\rho$) = 0.95(5) % (Table 4). The addition of the Curiw-Weiss term yielded the CW term to be zero within experimental error, indicating the magnetic isolation of the antiferromagnetic chains. The magnetization of **1** at 1.8 K and 5 T resulted in 1.68x10$^3$ emu mol$^{-1}$, approximately one third of the saturation moment expected for Cu(II) ions as a result of the antiferromagnetic interactions.

As previously stated, copper complexes containing bridging and terminal pyrazine molecules are uncommon in literature with even more limited data available on their magnetic properties. Compounds sharing similar components of pyrazine-bridged chains, dimers and 2D-systems with terminal pyrazines are presented due to the lack of information on the former. The following compounds involve a greater number of parameters and should be considered rough comparisons which are not structurally the same. Isolated **1** packs in 1D layers whereas $[Cu(HF_2)(pyz)_2]SbF_6$ packs in 2D square layers. The relative concavity of the susceptibility data of $[Cu(HF_2)(pyz)_2]SbF_6$ differs from **1** due to the interlayer exchange energy resulting in a rounded maxima observed at the higher temperature of 12.5 K and stronger interactions with $J$ = -13.5 K

**Table 3.** Hydrogen bonds and angles [Å and °].

| D-H...A | d(D-H) | d(H...A) | d(D...A) | <(DHA) |
|---|---|---|---|---|
| N(11)-H(11)...O(5)#3 | 0.75(3) | 2.31(3) | 2.959(3) | 146(3) |
| O(1W)-H(1A)...O(2W) | 0.77(3) | 1.94(3) | 2.711(2) | 176(3) |
| O(1W)-H(1B)...N(24)#4 | 0.76(3) | 2.04(3) | 2.701(3) | 147(3) |
| O(2W)-H(2A)...O(1)#5 | 0.77(4) | 2.03(4) | 2.793(3) | 169(3) |
| O(2W)-H(2B)...O(6)#4 | 0.70(4) | 2.26(4) | 2.946(3) | 171(4) |

Symmetry transformations used to generate equivalent atoms: #1 x,-y+3/2,z-1/2; #2 x,-y+3/2,z+1/2; #3 -x+1,y-1/2,-z+1/2; #4 x,-y+5/2,z+1/2; #5 -x+1,y-1/2,-z+3/2

The quasi-one-dimensional Heisenberg antiferromagnetic compound $Cu(pyz)(NO_3)_2$ consists of copper-pyrazine chains that exhibit a magnetic exchange of $J = -10.3$ K.[27] The nitrato ligands are able to directly donate electron density to the copper contributing to a stronger magnetic exchange whereas in compound **1** the electron donating group contribute through the pyridone ring first and then on to the Cu(II) ion.

known complex $[Cu(C_5H_4ClNO)_2(C_4H_4N_2)(H_2O)_2](ClO_4)_2$ will be most interesting.

**Table 4.** Magnetic susceptibility data for 1.

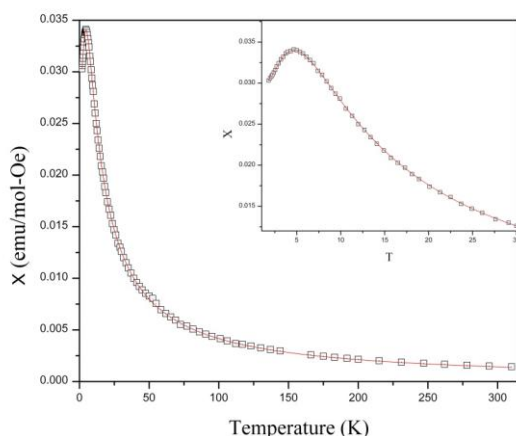| Model | C | J | θ | P |
|---|---|---|---|---|
| 1D-chain | 0.442 | -7.59(3) | | 1.01(7) |
| 1D-chain w/CW | 0.436(1) | -7.49(2) | -0.0002(0.3) | 0.95(5) |



**Figure 6.** $\chi_m$ vs. *T* plot for 1 in a 0.1 T field. The solid line corresponds to the prediction of the magnetic susceptibility of a 1D antiferromagnetic chain model with an exchange strength of -7.49(2) K and with a paramagnetic impurity term of 0.95(4). The inset shows an expansion of the region near the susceptibility maximum.

Exchange may also be affected by the terminal pyrazine ligand present. Both of these compounds exhibit drastically different lattices and so direct comparison of the exchange constants is of less value.

The intended goal was to create a homologous series that would allow for direct comparison of magnetic susceptibility and see what affects the observed exchange. Magnetic data for the chlorine-substituted literature compound $[Cu(C_5H_4ClNO)_2(C_4H_4N_2)(H_2O)_2](ClO_4)_2$,**Hiba! A könyvjelző nem létezik.** fit with a Curie-Weiss correction resulted in J = -9.90(7) K, CC = 0.446(1) emu(K) mol(Oe)$^{-1}$ and ρ = 1.6(2)%.[28] While **1** does not belong to the intended series, this compound suggests that the electron-withdrawing nitro group has a weakening effect on the strength of the magnetic exchange through the pyrazine ring in comparison to the complex with 5-Cl. The preliminary data supports the idea that the electron density at the copper ion has an effect on the exchange value. Efforts to isolate the intended linear chain compound $[Cu(C_5H_4N_2O_3)_2(C_4H_4N_2)(H_2O)_2](ClO_4)_2$ are in progress and comparison of its properties to **1** and the

## Supplementary data

CCDC 1418597 contains the supplementary crystallographic data for **1**. This data can be obtained free of charge via http://www.ccdc.cam.ac.uk/con-ts/retrieving.html, or from the Cambridge Crystallographic Data Centre, 12 Union Road, Cambridge CB2 1EZ, UK; fax: (+44) 1223-336-033; or email: deposit@ccdc.cam.ac.uk.

## References

[1] Miller, J. S., and M. D. *Magnetism: Molecules to Materials V.* Weinheim: Wiley-VCH, 2005. Print. (and previous volumes).

[2] Landee, C. P.; Turnbull, M. M., *J. Coord. Chem.,* **2014**, *67,* 375.

[3] Haynes, J.S.; Rettig ,S.J.; Sams, J.R.; Trotter, J.; Thompson, R.C. *Inorg. Chem.,* **1988**, *27,* 1237.

[4] Manson, J. L., Conner, M. M., Schlueter, J. A., McConnell, A. C., Southerland, H. I., Malfant, I., Lancaster, T., Blundell, S. J., Brooks, M. L., Pratt, F. L., Singleton, J., McDonald, R. S., Lee, C., Whangbo, M.-H. *Chem. Mater.,* **2008**, *20,* 7408.

[5] Butcher, R. T., Landee, C. P., Turnbull, M. M., Xiao, F. *Inorg. Chim. Acta,* **2008**, *361,* 3654.

[6] Manson, J. L., Schlueter, J. A., Funk, K. A., Southerland, H. I., Twamley, B., Lancaster, B. T., Blundell, S. J., Baker, P. J., Pratt, F. L., Singleton, J., McDonald, R. D., Goddard, P. A., Sengupta, P., Batista, C. D., Ding, L., Lee, C., Whangbo, M.-H., Franke, I., Cox, S., Baines, C., Trial, D., *J. Am. Chem. Soc.,* **2009**, *131,* 6733.

[7]Carlin, R. L., Magnetochemistry, Springer-Verlag, 1986.

[8]Schlueter, J. A., Park, H., Halder, G. J., Armand, W. R., Dunmars, C., Chapman, K. W., Manson, J. L., Singleton, J., McDonald, R., Plonczak, A., Kang, J., Lee, C., Whangbo, M.-H., Lancaster, T., Steele, A.J., Franke, I., Wright, J. M., Blundell, S. J., Pratt, F. L., DeGeorge, J., Turnbull, M. M., Landee, C. P., *Inorg. Chem.,* **2012**, *51*, 2121.

[9]Ikeda, M., Honda, Z., Sakai, M., Kiura, S., *Low Temp Phys*., **2013**, *170*, 296.

[10]Carranza, J., Jorunn, S., Brennan, C., Lloret, F., Cano, J., Julve, M., *Dalton Trans*., **2004**, 3997.

[11]Yuan, J.-X., Hu, M.-L., Cheng, Y.-Q., Chen, L.-C., Ng, S.W., *Acta Crystallogr*., *Sect.C: Struct. Crystallogr. Cryst. Chem.,* **2002**, *58*, 270.

[12]Perdih, F., *Monatsh Chem*. **2012**, *143*, 1011.

[13]Leznoff, D. B., Xue, B.-Y., Stevens, C. L., Storr, A., Thompson, R. C., Patrick, B. O., *Polyhedron.* **2001**, *20*, 1247.

[14]Manson, J. L., Huang, Q. Z., Lynn, J. W., Koo, H. J., Whangbo, M. H., Bateman, R., Otsuka, T., Wada, N., Argyriou, D. N., Miller, J. S., *J. Am. Chem. Soc*., **2001**, *123*, 162.

[15]CrysAlisPro Oxford Diffraction Ltd., Version 1.171.35.19 (release 27-10-2011 CrysAlis171.NET).

[16]Sheldrick, G. M., *Acta Cryst. A.,* **2008**, *64*, 112.

[17]Adamoicz, L., *Chem. Phys. Lett.,* **1989**, *161*, 73.

[18]Scanlan, M. J., Hillier, I. H., MacDowell, A., *J. Am. Chem. Soc.,* **1983**, *105*, 3568.

[19]Frank, J., Katrizky, A. R. *J. Chem. Soc., Perkin Trans.* 2., **1976**, *12*, 1428.

[20]Addison, A. W., Rao, T. N., Reedijk, J., van Rijn, J., Verschoor, G. C., *J. Chem. Soc., Dalton Trans.,* **1984**, 1349.

[21]Zhang, G.-F., She, J.-B., Dou, Y.-L., Fan, R. *Zeitschrift für Kristallographie - New Crystal Structures,* **2006,** *221,* 183.

[22]Forlani, L., Cristoni, G., Boga, C., Todesco, P. E., Del Vecchio, E., Selva S., Monari M. *Arkivoc* XI: 198

[23]de With, G., Harkema, S., Feil, D., *Acta Crystallogr., Sect.B: Struct. Crystallogr. Cryst. Chem*., **1976**, *32*, 3178.

[24]Otieno, T., Rettig, S. J., Thompson, R. C., Trotter, J. *Can. J. Chem.*, **1989**, *67*, 1964.

[25]Baillie, S. E., Blair, V. L., Blakemore, D. C., Hay, D., Kennedy, A. R., Pryde, D. C., Hevia, E., *Chem. Commun.,* **2012**, *48*, 1985.

[26]Bonner, J. C., Fischer, M. E., *Phys. Rev.* **1964**, *135*, A640.

[27]Günaydın-Şen, Ö., Lee, C., Tung, L. C., Chen, P., Turnbull, M. M., Landee, C. P., Wang, Y. J.; Whangbo, M.-H., Musfeldt, J. L., *Phys. Rev. B.,* **2010**, *81*, 104307.

[28]Selmani, V., Turnbull, M. M., Landee, C. P., unpublished results

# A NEW STRATEGY FOR THE SYNTHESIS OF 3-ACYLCOUMARIN USING NANO ZINC OXIDE AS AN EFFICIENT CATALYST

## Bita Baghernejad*

**Keywords:** Acyl coumarins, nanocatalysis, zinc oxide.

3-Acylcoumarins were obtained in high yields from *ortho*-hydroxybenzaldehydes and ethyl acetoacetate or ethyl benzoylacetate in acetonitrile in the presence of a catalytic amount of nano-ZnO.

* Corresponding Authors
　　E-Mail: bitabaghernejad@yahoo.com
　　Department of Chemistry, School of Sciences, Payame Noor University (PNU), Tehran, Iran

## Introduction

Coumarin and its derivatives form an elite class of compounds, occupying an important position in the realm of natural products and synthetic organic chemistry.[1] 3-Acyl-coumarins are important initial compounds for the synthesis of coumarins, which have attracted considerable attention from organic and medicinal chemists for many years as a large number of natural products contain this heterocyclic nucleus. Their applications range from additives in food, perfumes, cosmetics, pharmaceuticals to the preparation of insecticides,[1] optical brighteners,[2] dispersed fluorescent and tunable laser dyes.[3] Also, coumarins have varied bioactivities, for example, inhibition of platelet aggregation,[4] anticancer[5] and inhibition of steroid 5α-reductase.[6] Their properties turn coumarins very interesting targets to organic chemists, and several strategies for their synthesis were already developed. The last decade witnessed a series of publications on the development of synthetic protocols for this important heterocyclic scaffold. Thus, it is clearly evident that there is a need for the development of new and flexible protocols for the synthesis of coumarins.

Coumarins can be synthesized by various methods such as Pechmann,[7] Perkin,[8] Knoevenagel,[9] Reformatsky[10] and Witting[11] reactions. In 1898, Knoevenagel described the solution phase synthesis of coumarins by the condensation of malonic acid with *ortho*-hydroxyarylaldehydes.[9a] In our attempts to develop new catalyst systems, herein, we describe the use of this Knoevenagel condensation reaction to prepare 3-acylcoumarins, in high yields, in a mild and facile manner, in the presence of a catalytic amount of nano-ZnO.

## Experimental

### Chemicals and apparatus

All products are known compounds and were characterized by m.p., IR, ^{1}H NMR and GC/MS. Melting points were measured by using the capillary tube method with an electro thermal 9200 apparatus. ^{1}H NMR spectra were recorded on a Bruker AQS AVANCE-300 MHz spectrometer using TMS as an internal standard and CDCl₃ as a solvent. IR spectra were recorded on KBr disk using the FT-IR Bruker Tensor 27. GC/MS spectra were recorded on an Agilent Technologies 6890 network GC system and an Agilent 5973 network Mass selective detector. Thin layer chromatography (TLC) on commercial aluminum-backed plates of silica gel, 60 F254 was used to monitor the progress of reactions. All products were characterized by spectral and physical data.

### Preparation of the catalyst

Bulk zinc oxide was prepared by simple precipitation method wherein aqueous ammonia solution (30 %) was added drop-wise to zinc nitrate solution under vigorous stirring, till pH of solution reached 7.5-8. The white precipitate of $Zn(OH)_2$ was filtered and washed several times with distilled water till the washings were neutral. The precipitate was then dried overnight at 100 °C in an oven and calcined at 600 °C for 3 h. Nano zinc oxide catalyst was prepared by the gel combustion method as described by Riahi-Noori et al.[12] An appropriate molar ratio of citric acid and zinc nitrate (2:1) were mixed in a minimum amount of distilled water. The aqueous solution was homogenized and further concentrated on a hot plate to a viscous liquid, which was further heated at 100 °C for complete removal of water to obtain a dry mass. This mass was then further heated gradually till its combustion occurred giving a white fluffy powder. The powder obtained was annealed at 600 °C for 3h to give nano ZnO. The oxide was characterized by various analytical techniques to confirm its structural properties. External morphology and particle size of the catalyst was determined by TEM image (Figure 1). It is clear from TEM image that the zinc oxide has polymorphic geometry and the size of the particles is in the range of 50-70 nm.

### General synthetic procedure

A mixture of the appropriate benzaldehyde (1 mmol) and ethyl acetoacetate or ethyl benzoylacetate (1 mmol) and nano-ZnO (0.02 g) in MeCN (5 mL) was stirred at room temperature for 1.5 h. The progress of the reaction was monitored by TLC (EtOAc:hexane=1:2 as eluent). After completion of the reaction, the catalyst was filtered and the solvent was evaporated. The residue was recrystallized from EtOH to give the pure product (Scheme 1).
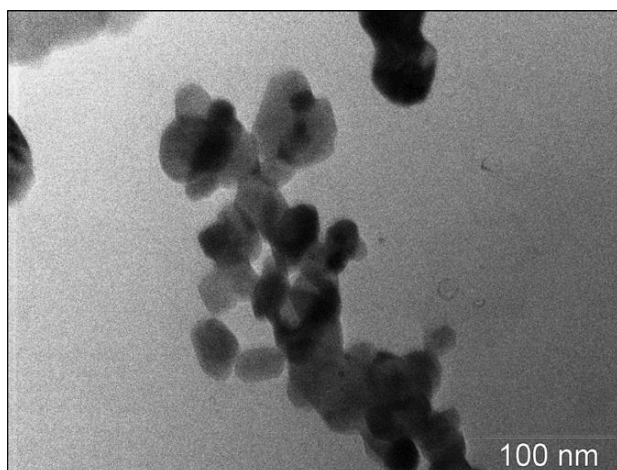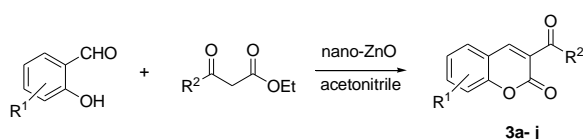
**Figure 1.** TEM image of nano zinc oxide at 100 nm.



**Scheme 1.** Synthesis of 3-acylcoumarins.

**3a**: m.p. 123 °C (Lit. 121/122 [13]).  IR (KBr): 1712, 1657, 1623, 1567, 1455, 1240, 1220, 980, 756 cm$^{-1}$; $^1$H NMR (CDCl$_3$, 500 MHz): δ = 2.76 (s, 3H, CH$_3$), 7.35-7.39 (m, 2H, Ar-H), 7.60-7.68 (m, 2H, Ar-H), 8.43 (s, 1H, CH).

**3e**: IR (KBr): 1746, 1670, 1611, 1500, 1357, 1200, 980, 831, 765 cm$^{-1}$; $^1$H NMR (CDCl$_3$, 500 MHz): δ = 2.77 (s, 3H, CH$_3$), 3.99 (s, 3H, OCH$_3$), 6.76 (d, J=2.30 Hz, 1H, Ar-H), 6.88 (q, J=3.70 Hz, 1H, Ar-H), 7.46 (d, J=8.70 Hz, 1H, Ar-H), 8.41 (s,1H, CH).

## Results and discussion

In this study, we have investigated the Knoevenagel condensation reaction to prepare 3-acylcoumarins and we set out for the synthesis of coumarins via condensation of *ortho*-hydroxybenzaldehydes with ethyl acetoacetate or ethyl benzoylacetate using nano-ZnO as an efficient catalyst at room temperature. To investigate the generality of this process, various salicylic aldehydes were reacted under similar conditions, allowing the easy synthesis of 3-acylcoumarins in good yields (Table 1). This one-pot procedure is convenient and straightforward with simple product isolation.  From Table 1, it can be observed that the reactions proceeded faster than the conventional methods and the yields were comparable.

To show the merits and advantages of using nano-ZnO as a catalyst, our method is compared with reported reactions (Table 2). The reaction results without catalyst decrease and the reaction time increases. This method is suitable for *ortho*-hydroxy benzaldehydes but the *ortho*-hydroxyaryl ketones were recovered and unchanged after the reaction.

## Conclusion

In conclusion, we have developed a simple and efficient synthesis of 3-acylcoumarins via Knoevenagel condensations in high yields and selectivities from *ortho*-hydroxybenzaldehydes using nano-ZnO as a catalyst under mild conditions at room temperature. Moreover the fast reaction time, simple experimental procedure, recyclability of the catalyst and high yields of the products is the main advantages. We believe our procedure will find important applications to the synthesis of coumarins.

**Table 1.** Synthesis of 3-acylcoumarins in the presence of nano-ZnO as a catalyst.

| Entry | R$^1$ | R$^2$ | Product | Yield (%) |
|-------|-------|-------|---------|-----------|
| 1 | H | CH$_3$ | 3a | 98 |
| 2 | 3-OH | CH$_3$ | 3b | 98 |
| 3 | 4-OH | CH$_3$ | 3c | 98 |
| 4 | 5-Br | CH$_3$ | 3d | 96 |
| 5 | 4-OMe | CH$_3$ | 3e | 98 |
| 6 | H | Ph | 3f | 95 |
| 7 | 3-OH | Ph | 3g | 96 |
| 8 | 4-OH | Ph | 3h | 96 |
| 9 | 5-Br | Ph | 3i | 93 |
| 10 | 4-OMe | Ph | 3j | 95 |

**Table 2.** Comparative efficiency of various catalysts for the synthesis of 3-acetylcoumarin (**3a**).

| Catalyst | Time | Yield (%) | Refer. |
|----------|------|-----------|--------|
| nano-ZnO | 1.5 h | 98 | This article |
| H$_{14}$[NaP$_5$W$_{30}$O$_{110}$] | 2 h | 98 | 14 |
| Piperidinium acetate | 2 h | 89 | 15 |
| none | 10 h | 90 | 16 |
| Piperidine | 2 h | 50 | 17 |
| [bmIm]OH | 15 min | 88 | 18 |

## References

[1]Kennedy, R. O., Zhorenes, R. D., *Coumarins. Biology, Applications and Mode of Action*, John Wiley and Sons, Chichester, **1997**.

[2]Zabradnik, M., *The Production and Application of Fluorescent Brightening Agents*, John Wiley and Sons, New York, **1992**.

[3]Murray, R. D. H., Mendez, J., Brown, S. A., *The Natural Coumarins: Occurrence, Chemistry and Biochemistry,* John Wiley and Sons, New York, **1982**.

[4](a) Mitra, A. K., De, K. Karchaudhuri, N., Misra, K., Mukopadhyay, A. K., *J. Indian Chem. Soc.,* **1998**, 75, 666. (b) Cravotto, G., Nano, M., Palmisano, G., Tagliapietra, S., *Tetrahedron: Asymmetry*, **2001**, *12*, 707.

[5]Wang, C. J.,  Hsieh, Y. J., Chu, C. Y., Lin, Y. L., Tseng, T. H., *Cancer Lett.*, **2002**, *183*, 163.

*Eur. Chem. Bull.,* **2016**, *5*(2), 60-62

DOI: 10.17628/ecb.2016.5.60-62

61

[6]Fan, G. J., Mar, W., Park, M. K., Wook Choi, E., Kim, K., Kim, S., *Bioorg. Med. Chem. Lett.*, **2001**, *11*, 2361.

[7]Sethna, S. M., Phadke, R., *Org. React.*, **1953**, *7*, 1.

[8]Donnelly, B. J., Donnelly, D. M. X., Sullivan, A. M. O., *Tetrahedron,* **1968**, *24*, 2617; Johnson, J. R., *Org. React.*, **1942**, *1*, 210.

[9](a)Jones, G*., Org. React.*, **1967**, *15*, 204 (b) Bigi, F., Chesini, L., Maggi, R., Sartori, G., *J. Org. Chem.*, **1999**, *64*, 1033.

[10]Shirner, R. L., *Org. React.*, **1942**, *1*, 1.

[11]Yavari, I., Hekmat-shoar, R., Zonuzi, A*., Tetrahedron Lett.*, **1998**, *39*, 2391.

[12]Kantam, M.L., Laha, S., Yadav, J., Sreedhar, B., *Tetrahedron Lett.*, 2006, *47*, 6213.

[13]Rahimizadeh, M., Bakhtiarpoor, Z., Eshghi, H., *Monatsh Chem.*, **2009**, *140*, 1465.

[14]Chen, X., Mao, S.S., *Chem. Rev.*, **2007**, *107*, 2891.

[15]Yu, H., Zhu, Y., Liu, C., *Chin. J. Catal.*, **2009**, *30*, 265.

[16]Wang, J., Sun, W., Zhang, Z., *J. Mol. Catal. A: Chem.*, **2007**, *27*, 84.

[17]Lin, C.H., Lin, Y.C., Chang, C.L., *React. Kinet. Catal. Lett.*, **2007**, *90*, 267.

[18]Sayilkan, F., Asilturk, M., Sener, S., *Turk. J. Chem.*, **2007**, *31*, 220.

# QUALITY ASSESSMENT AND CORRELATION ANALYSIS OF CHEMICAL DATA OF THE MIROSALA WELL WATER (KOSOVO)

## Fatbardh Gashi,[a] Naser Troni,[a] Fatmir Faiku,[a]* Albulena Thaqi[a] and Anilë Gashi[a]

**Keywords: :** Quality assessment; correlation coefficients; well water; Mirosala, statistical analysis.

In the present study, the chemical characteristics of the Mirosala well water are studied. Statistical analysis have been carried out by calculating of basic statistical parameters, anomalies (extremes and outliers) and correlation coefficients between different pairs of variables. The levels of some chemical parameters of the well water are compared with the World Health Organization directives for drinking water. From the results of field work and laboratory analyses it was found out that Mirosala well water fulfils the criteria set by the WHO. The statistical regression analysis showed that electrical conductivity is in high significant positive relationship with consumption of $KMnO_4$ and a moderately high positive correlation relationship with pH, $Fe^{2+}$, $NO_2^-$ and $Ca^{2+}$ (possible sign of lithology influence). No correlation was found with $SiO_2$, hardness, $NO_3^-$, $Cl^-$, $Mg^{2+}$ and $HCO_3^-$. In the water sample $S_3$ outlier value of $SiO_2$ (31.9 mg $L^{-1}$) was registered, as possible sign of lithology influence. The distribution of low pollutants has been described as lithologically and non lithologically controlled factor.

* Corresponding Authors
     E-Mail: f.faiku@hotmail.com
[a]     Department of Chemistry, Faculty of Natural Sciences, St. M. Teresa 10, University of Prishtina, Kosova

## Introduction

The sources of physico-chemical contamination of water bodies are numerous and include the land disposal of sewage effluents, sludge and solid waste, septic tank effluent, urban runoff and agricultural, mining and industrial practices.[1,2] Chemical contamination of drinking water is often considered a lower priority than microbial contamination by regulators, because adverse health effects from chemical contaminations are generally associated with long-term exposures, whereas the effects from microbial contamination are usually immediate.[3] The quality of drinking water is an issue of primary interest for the residents of the European Union.[4] In peat bogs, water flows freely in the active layer of water or acrotelm. Water storage is critical to the balance of water in peat swamps and at surrounding areas. Logging activity, agriculture, peat extraction and destruction of peat swamp drainage activity also give a negative effect and has a bad implication on the hydrology.[5] Decomposition of organic matter and pollution due to anthropogenic activity are the main sources of pollution of water.[6] Therefore, multidisciplinary collaborative research is essential for understanding the pollution processes.

As reported by Brils,[7] adequate water quality in Europe is one of the most eminent concerns for the future. Good management of natural and environmental waters will give results if leading institutions constantly monitor information about environmental situation. Therefore, seeing it as a challenge for environmental chemists, our goal is to determine the amount and nature of pollutants in the environment.



**Figure 1.** Area map with study location.

Until recently, the waters of Kosovo have been poorly investigated. Gashi et al[8] performed first step with investigation of the rivers Drini i Bardhë, Morava e Binçës, Lepenc and Sitnica, which are of supra-regional interest.

They performed investigations of mineralogical and geochemical composition and of contamination status of stream sediments of mentioned rivers of Kosovo. By comparing the concentrations of toxic elements with the existing criteria for sediment quality, it was found that two sites in Sitnica River are significantly polluted, especially locations in Fushë Kosova (Kosovo Polje) and in Mitrovica. This was assumed to be caused by Zn and Pb processing by flotation and Zn-electrolysis factory. In Morava e Binçës River, two sites were found to be polluted with Cd. The authors of that paper suggested future monitoring of sediments and possibly remediation

of Sitnica and Morava e Binçës rivers. As Drenica River is the most important tributary of Sitnica River, the current paper presents next step in detailed investigation and monitoring of Sitnica river watershed, which is most polluted river system in Kosovo.

Gashi et al[9-11] performed research of mass concentrations of ecotoxic metals viz. Cu(II), Pb(II), Cd(II), Zn(II) and Mn(II) in waters of four main rivers of Kosovo. The main goal of that work was to suggest to authorities concerned a monitoring network on main rivers of Kosovo (Drini i Bardhë, Morava e Binçës, Lepenc and Sitnica). The authors also aimed to suggest application of WFD (Water Framework Directive) in Kosovo as soon as possible and performed research could be the first step towards it, giving an opportunity to plan the monitoring network in which pollution locations will be highlighted. The authors highlighted two locations in Sitnica River as very polluted with ecotoxic elements and possible remediation by Kosovo authorities concerned was suggested. Troni et al.[12] compared the surface water quality in Kosovo in Lumbardhi River basin in the region of Peja. From chemical aspects are investigated some of main indicators pollution as: pH value (in situ), dissolved oxygen, lead, cadmium, copper, zinc, arsenic, cobalt, nickel, uranium, bromine, nitrites, etc. Based on Croatian standards for drinking water, the Lumbardhi River water was classified in first and second class according to the concentrations of zinc and cadmium. It is classified in the second, third and fourth class according to the concentrations of cuprum and lead. It was concluded that water resources of Kosovo's are endangered by antropogenic pollution.[13]

# Experimental

The aim of the current work is to perform, a systematic research of the well water quality in Mirosala village. Mirosala village located in the north-east of the town of Ferizaj, and is known for the hight water quality with curative properties. Mirosala water is the main source of water factory "Miros". Although there are more than 50 water quality parameters available, only 14 parameters are selected for our investigation. These parameters are: water temperature, conductivity, pH, consumption of $KMnO_4$, nitrate, nitrite, ammonia, etc. The results are interpreted using modern statistical methods that can be used to locate pollution sources.

### Sampling and sample preparation

For chemical analysis water samples are collected, during September 2014 to December 2014, in plastic bottles, previously rinsed three times with sampled water, and labelled with the date and the name of the sample. These samples are transferred to refrigerator (at 4 °C) for analysis in the laboratories. All tests are performed at least thrice to calculate the average value. Sampling, preservation and experimental procedure for the water samples are carried out according to the standard methods for examination of water.[14-17] Samples are preserved in refrigerator after treatment.

### Chemical characterization

Double distilled water was used in all experiments. All instruments are calibrated according to manufacturer's recommendations. Temperature of water was measured immediately after sampling. pH measurements were performed using pH/ion-meter of Hanna Instruments. Electrical conductivity (EC) is measured by InoLab WTW conductometer, chemical consumption of $KMnO_4$ using Thiemann Küebel volumetric method (boiling in acidic environment). Some of the physico-chemical parameters ($NO_2^-$, $NO_3^-$ and $NH_4^+$) are determined using UV-VIS spectrometry method using model Merck Spectroquant NOVA 60 Fotomoter.

### Statistical methods

Program Statistica 6.0[18] was used for the statistical calculations in this work, such as descriptive statistics, Pearson's correlation factor and two dimensional box plot diagrams for determination of anomalies (extremes and outliers) for solution data. Relationships between the observed variables were tested by means of correlation analysis. The level of significance was set at $p < 0.05$ for all statistical analyses. It was qualitatively assumed that the absolute values of $r$ between 0.3 and 0.7 indicate good association, and those between 0.7 and 1.0 strong association between elements.

# Results and discussions

The chemical parameters i.e. water temperature, EC, pH, total hardness, consumption of $KMnO_4$ and concentrations of $SiO_2$, $Fe^{2+}$, $Ca^{2+}$, $Mg^{2+}$, $Cl^-$, $NO_2^-$, $NO_3^-$, $NH_4^+$ and $HCO_3^-$ are presented in Table 1 and 2. The summary of descriptive statistics of the selected variables at water samples are presented in Table 3. For each variable, the values are given as arithmetic mean, geometric mean, median, minimal and maximal concentration, variance and standard deviation. Box-whiskers plot for measured variables are presented in Figure 2. Using experimental data (Table 1 and 2) and box plot approach of Tukey,[19] anomalous values (extremes and outliers) of 12 variables were determinate. Only ample $S_3$ showed an outlier parameter of $SiO_2$ (31.9 mg $L^{-1}$). Correlation Pearson's factor for 12 variables was calculated to see if some of the parameters were interrelated with each other and the results are presented in Table 4.

In the present study, the temperature varied from 14.8–16° C and there are higher than the temperatures (7.3°C) of both Rječina and Kupa karstic springs in Croatia, reported by Frančišković-Bilinski et al.[20] This is usual behavior of most of ground waters. As thermostat adjustment of the instrument for conductivity measurement was not done, temperature of water sample was measured and with approximate correction factor, $f$, which for water, in temperature range from 10 to 25°C, is $0.02°C^{-1}$, it was calculated to temperature of 20°C by Eqn. 1.

$$K_{20} = K_t \left[ 1 + f(20 - t) \right] \tag{1}$$

**Table 1.** Mean value of some physico-chemical parameters of the well water.

| Sample | Date | Water temp. º C | EC, µScm$^{-1}$ | pH | Hardness, °dH | Consumption of KMnO$_4$, mgL$^{-1}$ |
|--------|------|-----------------|-----------------|-----|---------------|-------------------------------------|
| S$_1$ | 11.09.14 | 16.0 | 478 | 7.93 | 10.08 | 12.64 |
| S$_2$ | 15.09.14 | 15.8 | 475 | 7.84 | 11.20 | 9.72 |
| S$_3$ | 10.12.14 | 14.8 | 471 | 7.90 | 11.77 | 9.03 |
| S$_4$ | 23.12.14 | 15.7 | 478 | 8.08 | 10.98 | 12.64 |
| S$_5$ | 26.12.14 | 15.5 | 476 | 8.06 | 11.20 | 10.53 |
| S$_6$ | 29.12.14 | 15.4 | 475 | 8.04 | 9.74 | 9.72 |

**Table 2.** Mean value of some chemical parameters of the well water.

| Sample | SiO$_2$, | Fe$^{2+}$ | Ca$^{2+}$ | Mg$^{2+}$ | Cl$^-$ | NO$_2^-$ | NO$_3^-$ | NH$_4^+$ | HCO$_3^-$ |
|--------|----------|-----------|-----------|-----------|--------|----------|----------|----------|-----------|
| S$_1$ | 19.2 | < 0.03 | 41.6 | 23.04 | 17.016 | 0.018 | 0.02 | n.d. | 286.7 |
| S$_2$ | 22.5 | 0.03 | 41.0 | 23.41 | 16.1 | 0.027 | 0.5 | n.d. | 284.5 |
| S$_3$ | 31.9 | 0.03 | 38.9 | 24.68 | 18.7 | 0.020 | 0.2 | n.d. | 280.6 |
| S$_4$ | 21.6 | 0.03 | 38.4 | 24.96 | 15.95 | 0.025 | 0.03 | n.d. | 274.5 |
| S$_5$ | 20.8 | 0.03 | 36.1 | 26.40 | 14.18 | 0.025 | 0.2 | n.d. | 335.2 |
| S$_6$ | 18.30 | 0.03 | 40.4 | 23.76 | 15.61 | 0.016 | 0.33 | n.d. | 366.0 |

Note: Concentration of ammonium ion was not determined. All concentrations are in mg L$^{-1}$.

**Table 3.** Basic statistical parameters for 12 variables in 6 water samples.

| Variable | Descriptive Statistics | | | | | | |
|----------|------|-----------|--------|---------|---------|----------|-----|
| | Mean | Geo. mean | Median | Minimum | Maximum | Variance | SD |
| EC, µS cm$^{-1}$ | 475.5000 | 475.4941 | 475.5000 | 471.0000 | 478.0000 | 6.700 | 2.58844 |
| pH | 7.9750 | 7.9745 | 7.9850 | 7.8400 | 8.0800 | 0.010 | 0.09834 |
| Hardness, tot., °dH | 10.8283 | 10.8054 | 11.0900 | 9.7400 | 11.7700 | 0.586 | 0.76557 |
| HCO$_3^-$, mg L$^{-1}$ | 304.5833 | 302.7988 | 285.6000 | 274.5000 | 366.0000 | 1382.550 | 37.18265 |
| C. of MnO$_4^-$, mg L$^{-1}$ | 10.7133 | 10.6208 | 10.1250 | 9.0300 | 12.6400 | 2.453 | 1.56619 |
| SiO$_2$, mg L$^{-1}$ | 22.3833 | 21.9975 | 21.2000 | 18.3000 | 31.9000 | 24.102 | 4.90934 |
| Fe$^{2+}$, mg L$^{-1}$ | 16.8583 | 0.1161 | 0.0300 | 0.0300 | 101.0000 | 1699.157 | 41.22083 |
| Ca$^{2+}$, mg L$^{-1}$ | 39.4033 | 39.3589 | 39.6500 | 36.1000 | 41.6000 | 4.121 | 2.02999 |
| Mg$^{2+}$, mg L$^{-1}$ | 24.3750 | 24.3493 | 24.2200 | 23.0400 | 26.4000 | 1.526 | 1.23512 |
| Cl$^-$, mg L$^{-1}$ | 16.2593 | 16.2017 | 16.0250 | 14.1800 | 18.7000 | 2.279 | 1.50968 |
| NO$_2^-$, mg L$^{-1}$ | 0.0218 | 0.0214 | 0.0225 | 0.0160 | 0.0270 | 0.000 | 0.00445 |
| NO$_3^-$, mg L$^{-1}$ | 0.2133 | 0.1258 | 0.2000 | 0.0200 | 0.5000 | 0.033 | 0.18283 |

**Table 4.** Matrix of correlation coefficients (*r*) of selected 12 variables.

| Variable | EC,µS cm$^{-1}$ | pH | Hardness total, °dH | HCO$_3^-$ mg L$^{-1}$ | C$_{KMnO4}$, mg L$^{-1}$ | SiO$_2$ mg L$^{-1}$ | Fe$^{2+}$ mg L$^{-1}$ | Ca$^{2+}$ mg L$^{-1}$ | Mg$^{2+}$ mg L$^{-1}$ | Cl$^-$ mg L$^{-1}$ | NO$_2^-$ mg L$^{-1}$ | NO$_3^-$ mg L$^{-1}$ |
|----------|------|------|------|------|------|------|------|------|------|------|------|------|
| EC, µScm$^{-1}$ | 1.00 | | | | | | | | | | | |
| pH | 0.44 | 1.00 | | | | | | | | | | |
| Hardness total, °dH | -0.52 | -0.29 | 1.00 | | | | | | | | | |
| HCO$_3^-$, mg L$^{-1}$ | -0.04 | 0.48 | -0.54 | 1.00 | | | | | | | | |
| C$_{KMnO4}$, mg L$^{-1}$ | 0.89 | 0.38 | -0.35 | -0.34 | 1.00 | | | | | | | |
| SiO$_2$, mg L$^{-1}$ | -0.81 | -0.44 | 0.80 | -0.49 | -0.51 | 1.00 | | | | | | |
| Fe$^{2+}$, mg L$^{-1}$ | 0.47 | -0.22 | -0.48 | -0.24 | 0.60 | -0.32 | 1.00 | | | | | |
| Ca$^{2+}$, mg L$^{-1}$ | 0.09 | -0.60 | -0.51 | -0.18 | 0.07 | -0.19 | 0.53 | 1.00 | | | | |
| Mg$^{2+}$, mg L$^{-1}$ | -0.09 | 0.59 | 0.52 | 0.19 | -0.08 | 0.19 | -0.53 | -1.00 | 1.00 | | | |
| Cl$^-$, mg L$^{-1}$ | -0.54 | -0.60 | 0.27 | -0.58 | -0.17 | 0.73 | 0.25 | 0.44 | -0.44 | 1.00 | | |
| NO$_2^-$, mg L$^{-1}$ | 0.15 | -0.08 | 0.65 | -0.42 | 0.05 | 0.11 | -0.42 | -0.41 | 0.42 | -0.36 | 1.00 | |
| NO$_3^-$, mg L$^{-1}$ | -0.46 | -0.46 | 0.11 | 0.30 | -0.77 | 0.05 | -0.52 | 0.21 | -0.20 | -0.16 | 0.23 | 1.00 |
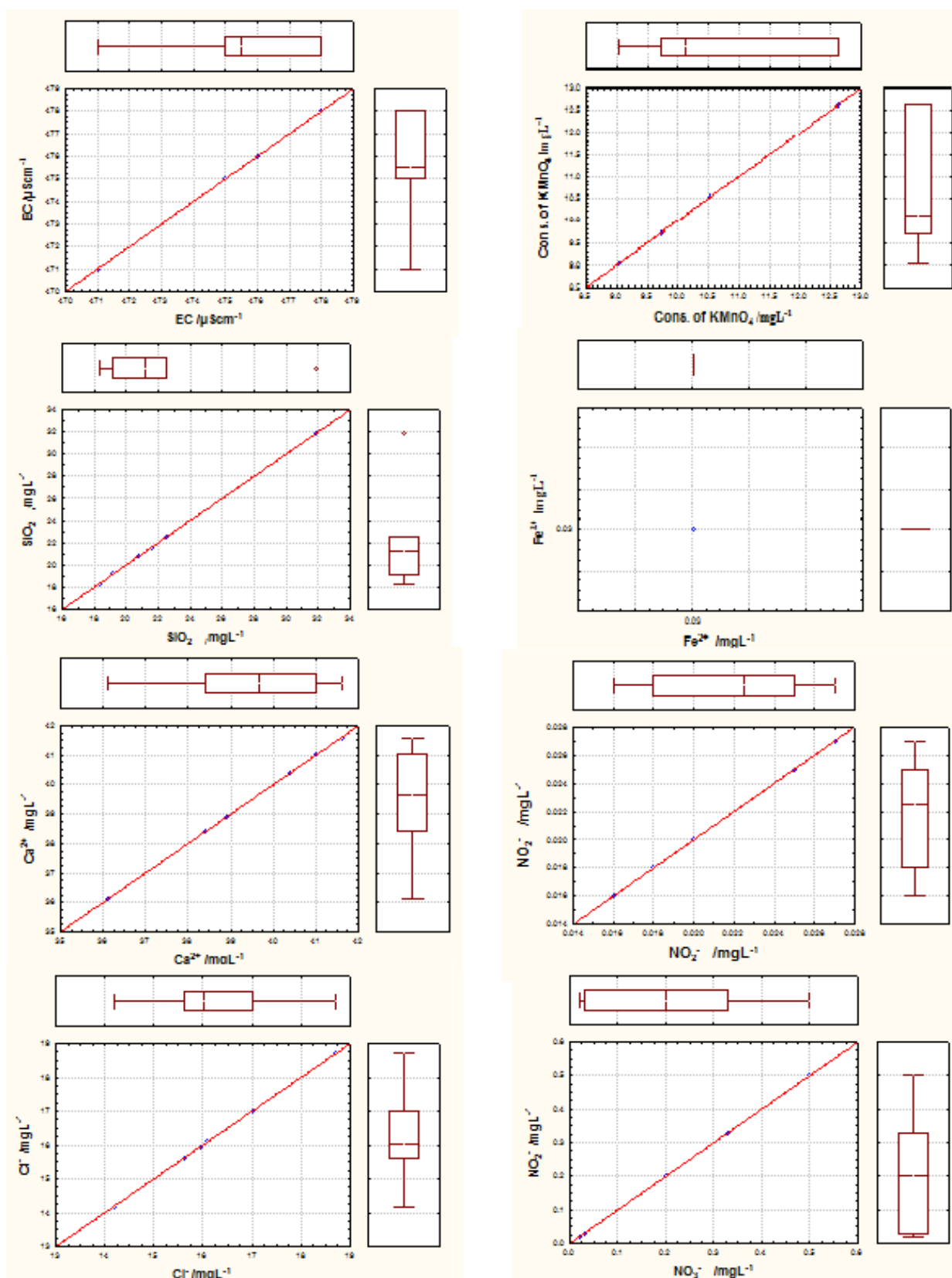
**Figure 2.** Scatter box plot diagrams of some measured variables

EC values are relatively high in the all samples. Lowest value of 471 µS cm$^{-1}$ is measured at station $S_3$ and the highest value of 478 µS cm$^{-1}$ which is measured at stations $S_1$ and $S_4$. All those values much higher of all values found in Kupa and Rječina rivers, Croatia, where values range from 200–250 µS cm$^{-1}$. The higher values of EC might be sign of natural pollution. Values of pH varied from 7.84-8.08, which is lower than the values found in water of karstic rivers of Croatia (pH up to 8.7). It could be due to composition of rocks in the area, as mentioned Croatian rivers are situated in karst, while our stations is situated in area of acid magmatic rocks. Total hardness, concentrations of $SiO_2$, $Fe^{2+}$, $Ca^{2+}$, $Mg^{2+}$, $Cl^-$, $NO_2^-$ and $NO_3^-$ and $HCO_3^-$ of the investigated samples showing that all water samples were in lower values. Concentrations of ammonium ion in all samples were under detection limit. Hydroxides, carbonates and hydrogen carbonates of alkali and earth alkaline metals, mainly Na, Ca and Mg make water alkaline. Macro components of ground water are controlled by weathering of rocks (water-rock interactions). Thus, prevailing components in water show the major impact of aquifer lithology. Chlorides in all samples were found to be under recommended WHO standards for drinking water (250 mg L$^{-1}$). Consumption of $KMnO_4$ was ranging from 9.03-12.64 and all samples were found to be in the limit of recommended WHO standard for drinking water (12 mg L$^{-1}$). Higher values of consumption of $KMnO_4$ might be sign of natural pollution.

**Statistical interpretation**

Basic statistical parameters (Mean, Geometric mean, Median, Minimum, Maximum, Variance and Standard deviation) for 12 parameters analyzed in 6 water samples are presented in Table 3. Based on the two dimensional scatter box plot diagrams (Figure 2) from 12 experimental data were constructed and anomalous values (extremes and outliers) have been determined. In the $S_3$ outlier value of $SiO_2$ (31.9 mgL$^{-1}$) was registered, possible sign of lithology influence. The statistical regression analysis has been found a highly useful technique for the linear correlating between various water parameters. The correlation coefficient indicates positive and negative significant correlation of variables with each other. Positive correlation mean one parameter increase with other parameters and negative correlation mean one parameter increase with other parameters decrease. In study period, EC (Table 4) showed high significant positive relationship with consumption of $KMnO_4$ and a moderately high positive correlation relationship with pH, $Fe^{2+}$, $NO_2^-$ and $Ca^{2+}$. No correlation was found with $SiO_2$, hardness, $NO_3^-$, $Cl^-$, $Mg^{2+}$ and $HCO_3^-$. pH showed a moderately high positive correlation relationship with $Mg^{2+}$, consumption of $KMnO_4$ and $HCO_3^-$. No correlation was found with $SiO_2$, hardness, $NO_3^-$, $NO_2^-$, $Ca^{2+}$ and $Cl^-$. Hardness showed high significant positive relationship with $SiO_2$, a moderately high positive correlation relationship with $Mg^{2+}$, $Cl^-$, $NO_3^-$, $NO_2^-$ (possible sign of lithology influence). No correlation was found with consumption of $KMnO_4$, $Fe^{2+}$, $Ca^{2+}$ and $HCO_3^-$. The bicarbonate ion showed a moderately high positive correlation relationship with $Mg^{2+}$ and $NO_3^-$. Consumption of $KMnO_4$ showed a moderately high positive correlation relationship with $Fe^{2+}$, $Ca^{2+}$ and $NO_2^-$. $SiO_2$ showed a high significant positive correlation relationship with $Cl^-$ and a moderately high positive correlation relationship with $Mg^{2+}$, $NO_3^-$ and $NO_2^-$ (possible sign of lithology influence). $Fe^{2+}$ showed a moderately high positive correlation relationship with $Ca^{2+}$ and $Cl^-$. $Ca^{2+}$ showed a moderately high positive correlation relationship with $NO_3^-$ and $Cl^-$. $Mg^{2+}$ showed a moderately high positive correlation relationship with $NO_2^-$. The nitrite ion showed a moderately high positive correlation relationship with $NO_3^-$.

**Conclusions**

In this study the assessment of water quality and correlation coefficients between different pairs of variables of the Mirosala well water has been investigated. Generally, ground waters of Kosovo are enriched in dissolved solids, as the consequence of aquifer lithology and residence time of ground water. From the results of field work and laboratory analyses it was found out that Mirosala well water fulfils the criteria set by the World Health Organization. In the $S_3$ outlier value of $SiO_2$ (31.9 mgL$^{-1}$) was registered, possible sign of lithology The statistical regression analysis showed that EC is in high significant positive relationship with consumption of $KMnO_4$ and a moderately high positive correlation relationship with pH, $Fe^{2+}$, $NO_2^-$ and $Ca^{2+}$ (possible sign of lithology influence). The distribution of low pollutants indicated lithology pollutants from waste water.

**References**

[1]Close, M., Dann, R., Ball, A, Pirie, R., Savill, M., Smith, Z., *J. Water Health*, **2008**, *6,* 83-98.

[2]Keswick, B. H., *Groundwater Pollution Microbiology*. John Wiley and Sons, New York, **1984,** 39-64.

[3]Thompson, T., Fawell, J., Kunikane, S., Jackson, D., Appleyard, S., Callan, P., Bartram, J., Kingston, P., *Chemical safety of drinking-water: Assessing priorities for risk management,* World Health Organization, **2007.**

[4]Chirila, E., Bari, T., Barbes, L., *Ovidius Univ. Ann. Chem.*, **2010**, *21,* 87-90.

[5]Hamilton, L. S., Forests and Water: A Thematic Study Prepared in the Framework of the Global Forest Resources Assessment. *1st Edn., Agriculture Organization of the United Nation, Rome,* **2008**, 78.

[6]Montgomery, J. M., *Water Treatment, Principles and Design,* John Wiley & Sons, New York, **1996,** 474.

[7]Brils, J., *Ann. Inst. Superiore Sanita.* **2008***, 44,* 218–223.

[8]Gashi, F., Franciskovic-Bilinski S., Bilinski, H., *Fres. Environ. Bull.*, **2009,** *18*. 1462-1471.

[9]Gashi, F., Frančišković-Bilinski, S., Bilinski, H., Troni, N., Bacaj, M., Jusufi, F., *Environ. Monit. Assess.,* **2011***, 175***,** 279–289.

[10]Gashi, F., Troni, N., Faiku, F., Laha, F., Haziri, A., Kastrati, I., Beshtica, E., Behrami, M., *Am. J.   Environ. Sci.,* **2013***, 9,* 142-155.

[11]Gashi, F., Troni, N., Hoti, R., Faiku, F., Ibrahimi, R., Laha, F., Kurteshi, K., Osmani S., Hoti, F., *Fresenius Environ. Bull.*, **2014,** *23,* 91-97.

[12]Troni, N., Faiku, F., Gashi, F., Hoti, R., Teneqja, V., Laha F., Berisha, R., *Int. J. Green Herbal Chem.,* **2013,** *2,* 203-207.

[13]Faiku, F., Hazir, I., Gashi, F., Troni, N., Haziri, I., *Eur. Chem. Bull.,* **2015,** *4,* 169-176.

[14]Skoog, D. A., West, D. M., Holler, F. J., *Fundamentals of Analytical Chemistry.* College Publishing, Philadelphia, **1992.**

[15]APHA, AWWA and WEF, *Standard Method for the Examination of water and waste water,* 20th ed. American Public Health Association, Washington D.C., **1998.**

[16]Alper, B., Abidin, K. Yuksel, K. B., *Water Air Soil Pollut*., **1998**, *149***,** 93–111.

[17]Dalmacija, B., *Water Quality Control in Towards of Quality Management, Text book,* Novi Sad, **2000. [**In Serbian].

[18]Stat Soft, Inc. STATISTICA (data analysis software system), ver. 6. http://www.statsoft.com. **2001.**

[19]Tukey, J. W., *Exploratory data analysis,* Addison-Wesley. Reading, **1977.**

[20]Frančišković-Bilinski, S., Cuculić, V., Bilinski, H., Häusler, H., Stadler, Ph., *Chem. Erde,* **2013,** *73,* 293–308.

# ASSESSMENT OF PESTICIDES IN ENVIRONMENTAL SAMPLES USING VOLTAMMETRIC MOLECULAR IMPRINTED BASED SENSORS: A REVIEW

## Ayman. H. Kamel,[a]* Hend. Z. Yamani,[b] Nardine Safwat,[b] and Hoda R. Galal[c]

**Keywords:** Molecular imprinting polymer (MIP); voltammetric sensors; pesticides; environmental samples

The increased concern about toxic effects of pesticide exposure led to the necessity of its monitoring using rapid, sensitive and selective analytical tools because traditional instrumental techniques are often time-consuming, labor intensive and need tedious prior separation or purification steps. The electrochemical sensors can overcome disadvantages of the traditional techniques, MIP-based sensors offer a high degree of selectivity in binding target analytes in the presence of their interferents make them ideal for determination of pesticides in complex environmental samples. This review provides a general overview of MIP-based sensors in the assessment of pesticides in environmental samples using voltammetry as transduction mechanism.

Corresponding Authors
E-Mail: ahkamel76@sci.asu.edu.eg; ahkamel76@yahoo.com
Tel: (+2) 01000361328
[a]    Chemistry Department, Faculty of Science, Ain Shams University, Abbassia, 11566 Cairo, Egypt
[b]    Pharmaceutical Analytical Chemistry Department, Faculty of Pharmacy, Ain Shams University, Cairo, Egypt
[c]    National Research Center (NRC), Dokki, Giza,14211 Egypt

## Introduction

Pesticides are widely used in agricultural production to decrease losses by pests and to improve yield as well as the quality of the produce.[1] The massive use of pesticide has raised serious concerns not only about potential effects on human health (carcinogenicity, neurotoxicity, genotoxicity, birth defects and fetal death),[2] and animal wealth but also about its impact on the environment and sensitive ecosystems (water, soil and air contamination, toxic effects on non-target organisms).[3,4] In recent years, the increased concerns about dangerous and toxic effects of pesticides has led to the necessity of its monitoring. Due to a large variety of pesticides and required environmental analyzes, the need for low-cost, rapid, sensitive and selective analysis is continuously increasing.

There are various analytical methods such as LC-MS, GC-MS[5]HPLC,[6] GC[7] TLC,[8] CE,[9] spectrophotometry,[10] and fluorimetry,[11] for pesticides assessment in environmental samples. However, traditional instrumental analytical techniques are often time-consuming, labor intensive and need tedious prior separation or purification steps and expensive instrumentation. Electrochemical sensors are well suited for the pesticide analysis in the environment. These offer good sensitivity which allows low LOD, fast response which is useful for flow analysis, portability, simplicity in construction and use, miniaturization and low fabrication cost.[12]

Electrochemical sensors can be divided into three types: potentiometric, voltammetric and conductometric sensors.[13] All voltammetric techniques involve the application of a potential ($E$) to an electrode and recording the resulting current ($I$) flowing through the electrochemical cell as a function of the concentration of the analyte. In many cases, the applied potential is varied or the current is monitored over a period of time ($t$). Thus, all voltammetric techniques are some function of $E$, $I$, and $t$.

There are various types of voltammetric techniques such as (*i*) Cyclic voltammetry (CV) which is based on varying the applied potential at a working electrode in both forward and reverse directions (at same scan rate) while monitoring the current. (*ii*) Normal Pulse Voltammetry (NPV) that uses a series of potential pulses of increasing amplitude and the current is then measured near the end of each pulse. (*iii*) Differential Pulse Voltammetry (DPV) that scans a series of pulses at a fixed potential pulse of small amplitude (10 to 100 mV) and is superimposed on a slowly changing base potential. The current is measured at two points for each pulse, the first point just before the application of the pulse and the second at the end of the pulse. (*iv*) Square wave voltammetry (SWV) that consists of a symmetrical square-wave pulse of amplitude superimposed on a staircase waveform of step height, where the forward pulse of the square wave coincides with the staircase step. The net current is obtained by taking the difference between the forward and reverse currents and is centered on the redox potential. (*v*) Anodic stripping voltammetry (ASV) which is a widely used for trace metal determination and has a practical detection limit in the part-per-trillion range. (*vi*) Cathodic stripping voltammetry (CSV) that is used to determine substances that form insoluble salts with mercurous ions. Adsorptive stripping voltammetry (AdSV) is quite similar to anodic and cathodic stripping methods. The primary difference is that the pre-concentration step of the analyte is achieved by adsorption on the electrode surface or by specific reactions at chemically modified electrodes rather than accumulation by electrolysis.[14]

Voltammetric sensors continue to be the most popular ones among electrochemical sensors due to their simplicity, ease of production and the low cost.

The application of MIP in sensor development has continued to flourish. This is reflected by the rapid and enormous growth in the number of published papers concerning MIP-based electrochemical sensors. One of the main reasons for this is the high degree of selectivity in binding target analytes in the presence of their interferents making them ideal for determination of pollutants in complex environmental samples.

Molecular imprinting technology (MIT) is a versatile and promising technique based on the template-assisted synthesis with specific memory toward the template. This technology depends on the formation of a complex between an analyte (template) and a functional monomer in the presence of a cross-linking agent After polymerization process, the template is removed from the formed three-dimensional polymer network leaving specific recognition cavities complementary in shape, size and chemical functionality to the template molecule. Usually, intermolecular interactions like hydrogen bonds, dipole–dipole and ionic interactions between the template molecule and functional groups present in the polymer matrix drive the molecular recognition phenomena. Thus, the resultant polymer recognizes and binds selectively the template molecules.[15]

The review provides a general overview of MIPs field discussing first methods of MIP preparation and then dealing with applications of MIP-based sensors in the assessment of environmental samples using voltammetry as transduction mechanism.

## Synthesis of molecularly imprinted beads

The imprinting approach can be classified into two wide branches based on the matrix material used for template incorporation. These two main approaches are discriminated by the use of organic and inorganic matrices.[16]

### Organic Matrix

Organic polymers used as the imprinting matrix are further divided into covalent and non-covalent ones based on of the type of the binding between template and polymer matrix.

*Covalent approach*

The template binds to the matrix by covalent bonds, and the molecular recognition is achieved by formation and cleavage of these bonds.[17] An advantage of this approach is the creation of a strong and specific affinity towards the template. However, this strong binding is sometimes considered as a disadvantage because of the difficulty in template removal. For this reason, this approach is considered more suitable for catalytic[18] and separation purposes[19] than for sensing applications.[20]

*Non-covalent approach*

The other approach is non-covalent binding between template and monomer in the organic matrix. The main interactions include van der Waals forces, hydrogen bonding, ionic interactions, $\pi$-$\pi$ interactions and hydrophobic forces.[21] The most successful and widely used combination is methacrylic acid (MAA) as a functional monomer and ethylene glycol dimethacrylate (EGDMA) as a cross-linking agent. MAA is the most popular functional monomer because it can form hydrogen bonds with a wide variety of functional groups on a template.[22] Most commonly, polymerization is initiated either by adding free radical initiator (AIBN, 2,2-azo-bis-isobutyronitrile, or benzoyl peroxide, BPO) or induced photochemically at low temperatures or thermochemically at temperatures higher than 60 °C.[23]

The previous two approaches have advantages and disadvantages. In covalent approach, strong binding results in highly selective imprinting sites However, it suffers from a major drawback which is low reversibility and slow rate of template removal. In the non-covalent approach, specificity of binding sites strongly depends on the amount of functional monomer The affinity the template increases by increasing the amount of functional monomer On the other hand, excess functional monomer molecules in the matrix create a larger number of non-specific binding sites, thus lowering the selectivity of the imprinted polymer . Because of these problems active search is conducted to find alternative imprinting approaches[24] or modify the classical ones.

### Inorganic matrix

Organic MIPs suffer from certain drawbacks arising from their physicochemical properties such as rigidity, stability, penetrability and aging. A specific example to this is the swelling of the organic polymer when it is immersed in the solution.[25,26] Moreover, a small amount of the template usually remains in the imprinted polymer in spite of the careful extraction step . In addition to that, the leakage of the template, when solvents are exchanged, may produce a false response in sensor applications. Fortunately, inorganic materials posses the ability to overcome such disadvantages of the organic MIPs.

*Sol-gel approach*

Instead of organic monomer inorganic precursors are used to form siloxane based polymers via a sol-gel imprinting process that incorporate template molecules. Water and low molecular weight alkoxides are the most commonly used sol-gel precursors. Generally, a catalyst is needed to accelerate the polymerization process which is based on hydrolysis followed by condensation step. The hydrolysis step can be promoted by acid catalysis while the condensation step can be accelerated by basic catalysis.[27] Careful control of the sol-gel reaction parameters allows obtaining various imprinting forms (powders, thin films, monoliths, etc.). The sol-gel process provides a convenient method for the production of organically modified surface by incorporating alkoxysilane monomers that contain desirable functional groups in the starting polymerization mixture.[28,29]

*Liquid phase deposition approach (LPD)*

The LPD is an aqueous method for the preparation of metal oxide thin films from metal fluoro complexes $(MF_n)^{(m-n)}$ (where *m* is the cation charge and *n* is the number of fluoro ligands) whose hydrolysis in water is modulated by the addition of boric acid $(H_3BO_3)$ or aluminum metal.[30,31] This process is assumed to proceed according to the following reactions:

$$[MF_n]^{(m-n)}(aq) + m/2H_2O \rightarrow MO_{m\backslash2}\ (s) + nF^-\ (aq) + mH^+\ (aq) \quad (1)$$

$$H_3BO_3(aq) + 4HF\ (aq) \rightarrow BF_4^-\ (aq) + H_3O^+\ (aq) + 2H_2O \quad (2)$$
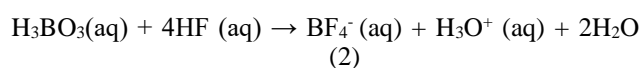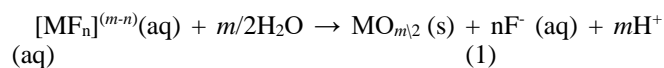
$H_3BO_3$ is used to promote the reaction (1), by shifting the equilibrium of equation (2) to the right.[32] As a result, very stable $BF_4^-$ anion is produced and the metal oxide thin film is then formed on the substrate. The advantage of LPD method lies in its simplicity, low cost and uniform film fabrication. For molecular imprinting, mainly $TiO_2$ films have been prepared from ammonium hexafluoro titanate (IV) $([NH_4]_2TiF_6)$ and boric acid in solution.[33,34] The ligand exchange hydrolysis of $[TiF_6]^{2-}$ has been proposed in the equilibrium reaction (3).[35]

$$[TiF_6]^{2-}(aq)\ +\ xH_2O \rightarrow\ [TiF_{6-x}(OH)_x]^{2-}(aq) +\ xHF\ (aq) \quad (3)$$
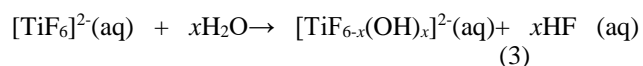
## Polymerization options[16]

### Free-radical polymerization

Vinyl based monomers and crosslinkers are commonly used in this type of polymerization. The process involves three steps; initiation to activate the monomers, propagation to grow the active chain, and termination of the active chain to form the final polymer chain. The external initiator is usually added to activate the polymerization process either by thermal or radiation process. The reactor is usually sealed under inert gas to avoid termination or radical species.

### Condensation polymerization

Reactive chemical functional groups of monomers react with each other to form new bonds. By-products such as water or hydrogen chloride may be produced from these reactions.

### Electro-polymerization

In an electrochemical polymerization, the monomer is oxidized at the surface of an electrode, by an anodic potential (oxidation) that is applied to it. This process is carried out in an appropriate solvent containing the desired anionic doping electrolyte. The solvent and electrolyte should be stable at the oxidation potential of the monomer and able to provide an ionically conductive medium. Upon the initial oxidation, the radical cation of the monomer is formed then it reacts with other monomers forming oligomeric products. The anode can be fabricated of a variety of materials including platinum, gold, glassy carbon, and tin or indium-tin oxide coated glass.

Electro-polymerization can be considered the most attractive procedure. This is because thickness, viscoelastic properties, porosity, and morphology of the resulting film can be easily controlled by selecting the suitable experimental conditions (e.g., the amount of charge transferred, solution pH, and the nature of the solvent, the supporting electrolyte, the functional monomer, and the cross-linking monomer).[36]

## Configuration of matrix[37]

### Bulk

The synthesis is performed using one pot method, where all the ingredients are mixed together. The MIP obtained is in the form of a block, having the shape of the reaction chamber. The bulk MIPs usually need further sample pre-processing by grinding and sieving to obtain micrometer-sized particles. A major disadvantage of this process is that the particles of MIP obtained are of irregular shape and size. Practically, the binding sites are distributed throughout the ground particles and a large number of them remain in the core of the matrix. Some of the imprinting sites may lost as a result of the grinding process thereby the final yield of the MIP is expected to be low.

### Monoliths

This format can be prepared by grafting of MIPs layer on a performed particle, utilizing a surface bond radical initiator.[38,39] In this method, azo–initiators or specifically known as iniferters are first immobilized on the surface of the performed particles. An iniferter is an initiator for free radical polymerization.

### Membranes

MIPs can be fabricated on thin film layers or membranes by three approaches, sandwiching or in situ cross-linking method, phase inversion -method or composite blending method.

## Applications of voltammetric MIP-based sensors in pesticides analysis

The application of molecularly imprinted polymers (MIPs) has attracted much attention as reflected by innumerable references in the literature. A survey of literature in last ten years (2006-2015) about applications of voltammetric MIP-based sensors in pesticides analysis was summarized in the following table.[40-87]

**Table 1.** Properties of voltammetric MIP-based sensors used in pesticides analysis

| Pesticide | Monomer/crosslinker /initiator | Porogen | Conditions of MIP preparation | Extraction conditions | Transduct ion method | Solution for analyte binding | Linear concentratio n range | LOD |
|---|---|---|---|---|---|---|---|---|
| 4-Aminophenol | MAA/TRIM/AIBN/ hemin[40] | Dimethylsulfoxide, acetonitrile | Heating at 60 ºC for 9 h | Methanol: acetic acid (9: 1, v/v) | Ampero-metry | 0.05 M TRIS buffer (pH 7.0) contg. 100 µM $H_2O_2$. | 9.8-79.4 µM | 3 µM |
| Acephate | o-Phenylenediamine[41] | Phosphate buffer (pH 5) | Potentiody-namic −0.2 - 1.0 V vs Ag/AgCl | Methanol, acetic acid (9:1, v/v) | DPV | 0.1 M phosphate buffer (pH 5) contg. 5 M $K_3[Fe(CN)_6]$, 0.2 M KCl | $5× 10^{-7}$ - $1× 10^{-4}$ M | $1.3× 10^{-7}$ M |
|  | 4-(Dimethoxyphospho-rothioylamino)buta-noic acid/3-amino-propyltriethoxysilane/ tetraethoxysilane[42] | Tetrahydrofuran | Potentiody-namic −0.4 - +0.8 V vs SCE | Methanol, acetic acid (9:1, v/v) | DPV | $K_3Fe(CN)_6$/ $K_4Fe(CN)_6$ | $1×10^{-4}$- $1× 10^{-10}$ M | $6.81× 10^{-11}$ M |
| Atrazine | Acetic acid/ thio-phene/3,4-ethylene-dioxythiophene[43] | Dichloromethane | Potentiosta-tic at 1.45 V vs. Pt | Methanol: acetic acid (0.7: 0.3, v/v) | CV | 0.1 M $Bu_4NO_3SCF_3$ in $CH_2Cl_2$ | $10^{-9}$-$1.5x10^{-2}$ M | $10^{-7}$ M |
|  | o-Phenylenediamine[44] | 0.1 M Phosphate buffer (pH 7.4) | Potentiody-namic 0–0.8 V vs SCE | Methanol, acetic acid (9:1, v/v) | DPV | $K_3[Fe(CN)_6]$/ $K_4[Fe(CN)_6]$, 0.1 M KCl | $5× 10^{-9}$- $1.4 × 10^{-7}$ M | $1× 10^{-9}$ M |
| Chlorpyrifos | 4-Aminothiophe-nol/AuNPs[45] | 0.05 M Phosphate buffer (pH = 6.86), 0.1 M KCl | Potentiody-namic, -0.2 to +0.6 V vs. Ag/AgCl | 0.5 M HCl | CV | 0.05 M phos-phate buffer (pH = 6.86) contg. 0.1 M KCl | 0.5-10 µM | 0.3 µM |
| Cyanazine | AA/EGDMA/AIBN[46] | Toluene | Heating at 60 °C for 16 h | MeOH/ace-tic acid (9:1, v/v) (Soxhlet extraction) | DPV | 0.1 M HCl (pH 2.7) | 5–1000 nM | 3.2 nM |
| Carbaryl | p-Aminothiophenol/ tetrabutylammonium perchlorate[47] | Ethanol | Potentiody-namic, -0.2 −1.4 V vs SCE | 20 % EtOH, 0.2 M HCl | DPV | 5mM $K_3Fe(CN)_6$/ $K_4Fe(CN)_6$, 0.2 M KCl | 0.03 µM – 6 µM | 8 nM |
| Dimethoate | o-Phenylenediami-ne/Au NPs[48] | Acetate buffer (pH = 5.2) | Potentiody-namic 0 to 0.8 V vs. SCE | Ethanol | Ampero-metry | Water | 1-1000 ng $mL^{-1}$, 1-50 µg $mL^{-1}$ | 0.5 ng $mL^{-1}$ |
| 2,4-Dichlorophe-noxyacetic acid | Pyrrole[49] | 0.05 M Phosphate buffer (pH = 6.86), 0.1 M KCl | Potentiody-namic, -1.3 to +1.0 V vs. Ag/AgCl | Overoxi-dation at 1.3 V vs. Ag/AgCl in 0.2 M $Na_2HPO_4$ | CV | 0. 05 M phosphate buffer (pH = 6.86), 0.1 M KCl | 1-10 µM | 0.83 µM |
|  | Pyrrole[50] | 15 mM Cetyltri-methylammonium bromide | Chemical oxidation | Ethanol: acetic acid (99: 1, v,v) | Ampero-metry | 50 mM phosphate buffer (pH = 6.8) | 0.1-8 µM | 100 nM |
| 2,4-Dichlorophe-noxybutyric acid | (Co(III) tetrakis(o-aminophenyl)por-phyrin[51] | 0.1 M $Bu_4NPF_6$, acetonitrile | Potentiody-namic -0.1 to +1.0 V vs. Pt | MeCN, MeOH | Ampero-metry | 0.1 M $Bu_4NPF_6$ in MeCN | 200 µM-2 mM | 40 µM |
| 4,6-Dinitro-o-cresol | o-Phenylenediami-ne/aniline[52] | 0.2 M Sulfuric acid: methanol (1:1, v/v) | Potentiody-namic -0.1 to +1.0 V vs. Ag/AgCl | Water: methanol (6: 4, v/v) | SWV | 0.04 M Britton–Robin-son buffer (pH 3) contg. 10 % MeOH | 0.8 µM-0.1 mM | 0.2 µM |
| O,O-dimethyl-(2,4-dichlorophe-noxyacetoxyl)-(3-nitrobenzyl)meth-anephosphonate | p-tert-Butylcalix[6]-arene/$TiO_2$[53] | - | Condensa-tion | Dichloro-methane | DPV | 0.1 M phosphate buffer (pH = 5.5) | 0.1-50 µM | 0.04 µM |
| Diuron | MAA/ TRIM/AIBN[54] | Acetonitrile | Heating at 60 °C for 24 h | Methanol, acetic acid (9:1, v/v) | SWV | Water, ethanol (20:1, v/v) | $5.2 ×10^8$ - $1.25× 10^6$ M | $9×10^9$ M |
| Fenitrothion | Ni(II)-phthalocya-nine[55] | 0.01 M Sodium hydroxide | Potentiody-namic -0.1 to +0.6 V vs. Ag/AgCl | 0.1 M $NH_4Cl$/$NH_4OH$ (pH 9.5) | SWV | 1 M NaCl | 3 µM-0.1 mM | 0.8 µM |
| Hexazinone | AA, 2-vinylpyridi-ne/MAA/EGDMA/ AIBN[56] | Dichloromethane | Heating at 60 °C for 24 h | Methanol, acetic acid (9:1, v/v) | DPAdCSV | Hydrochloric acid (pH 2.5) | $1.9×10^{-11}$- $1.1× 10^{-10}$M | $2.6× 10^{-12}$M |
| Imidacloprid | o-Phenylenediamine[57] | Acetate buffer (pH 5.2) | Potentiody-namic −0.2 - 0.8V vs SCE | 0.5 M HCl | CV | 0.1 M phosphate buffer (pH 7) | $7.5×10^{-7}$ - $7×10^{-5}$ M | $4×10^{-7}$ M |

| | | | | | | | | |
|---|---|---|---|---|---|---|---|---|
| **Isocarbophos** | o-Phenylenediamine, gallic acid/ m-aminobenzoic acid[58] | 0.02 M Phosphate buffer (pH 4) , 0.2 M KCl | Potentiodynamic −0.4 - 0.8V vs SCE | Distilled water | CV | 2 mM $K_3Fe(CN)_6/K_4Fe(CN)_6$ (1:1) | $7.5 \times 10^{-8}$ - $5 \times 10^{-5}$ M $5 \times 10^{-5}$- $1 \times 10^{-4}$ M | $2.01 \times 10^{-8}$ M |
| **Metolcarb** | 2-Amiothiophenol[59] | 0.1 M Hydrochloric acid, ethanol | Potentiostatic at-0.6 V vs. SCE, potentiodynamic -0.2 to +1.4 V | Potentiostaticly at 0.6 V for 600 s in 1 M HCl | Chrono-amperometry | 0.001 M $K_3[Fe(CN)_6]$ containing 0.001 M $KNO_3$ | 0.5-3.5 μM | 13.4 nM |
| **Metamitron** | *o*-Phenylenediamine/aniline[60] | 0.1 M Sulfuric acid | Potentiodynamic -0.1 to +1.35 V vs. Ag/AgCl | 1 M $NH_4Cl$/ $NH_4OH$ (pH 10) | SWV | 0.04 M Britton–Robinson buffer (pH = 1.8) | 1 μM–0.1 mM | 0.27 μM |
| **Methyl parathion** | Tetraethylorthosilicate and vinyltriethoxy-silane[61] | Ethanol, 0.2 M KCl | Potentiostaticat -1.80 V | Ethanol | SWV | phosphate buffer (pH 5.9) | $10^{-8}$-$10^{-5}$ M | $8.9 \times 10^{-9}$ M |
| | 3-Mercaptopropionic acid/$Fe_3O_4$/Au NPs/ polyethylenediamine[62] | Ethanol | - | CV for 50 segments (25 cycles) | DPV | phosphate buffer (pH 5.5) | $2 \times 10^{-7}$-$1 \times 10^{-4}$ M | $1 \times 10^{-7}$ M |
| | Quercetin/ resorcinol/ $KClO_4$[63] | 0.2 M Acetic acid buffer (pH 5.8) | Potentiodynamic −0.2-0.9V vs Ag/AgCl | Ethanol acidic solution (pH 5.2) | CV | $5 \times 10^{-3}$ M $K_3[Fe(CN)_6]$, 0.1 M $NaClO_4$ | $7 \times 10^{-8}$ M- $1 \times 10^{-6}$ M | $3.4 \times 10^{-10}$ M |
| | Phenol[64] | 0.13 M Phosphate buffer (pH 8) | Potentiodynamic 0.3-1.2V vs Ag/AgCl | 0.1 M Sulfuric acid | CV | 5 M $K_3[Fe(CN)_6]$ contg. 0.1 M KCl | 0.1 - 10 μg mL$^{-1}$ | 0.01 μg mL$^{-1}$. |
| | AA/ EGDMA/AIBN[65] | Chloroform | Heating at 60 °C | Ethanol | DPV | 0.2 M Phosphate buffer ( pH 7) | $5 \times 10^{-9}$ - $1 \times 10^{-5}$ M | $2 \times 10^{-9}$ M |
| | AA/ EGDMA/AIBN[66] | Dimethyl formamide | Heating at 60 °C | Methanol, acetic acid (9:1, v/v) | DPV | 0.1 M Phosphate buffer ( pH 5) | $2 \times 10^{-7}$ - $1 \times 10^{-5}$ M | $6.7 \times 10^{-8}$ M |
| **4-nitrophenol** | Carbazole[67] | Boron trifluoride diethyl etherate | Potentiodynamic range 0-1.4 V vs SCE | - | CV | Acetate buffer (pH 4.6 ) | $8 \times 10^{-7}$- $2 \times 10^{-5}$ M | 0.062 M |
| | MAA/EGDMA/ AIBN[68] | Dimethyl formamide | Heating at 65 ºC for 24 h | Methanol, acetic acid (4:1, v/v) | DPV | Phosphate buffer (pH 7) | 0.01 μM - 100 μM 200 μM - 1000 μM | 5 nM |
| | MAA/EDMA/AIBN[76] | Chloroform | Heating at 60 ºC for 24 h | Methanol (Soxhlet extraction) | DPV | Acetate buffer (pH 4.5) | $8 \times 10^{-9}$- $5 \times 10^{-6}$ M | $3 \times 10^{-9}$ M |
| | 1-Dodecanethiol/p-toluenethiol[77] | Dimethyl formamide | Potentiodynamic 0.6 - −0.7 V vs Ag/AgCl | 0.1 M Phosphate buffer (pH 6) | DPV | 0.1 M Phosphate buffer (pH 6) | $2.5 \times 10^{-8}$ M– $1 \times 10^{-6}$ M $1 \times 10^{-6}$ M– $3 \times 10^{-4}$ M | $2 \times 10^{-8}$ M |
| **Parathion** | p-tert-Butylcalix[6]-arene/$TiO_2$[69] | - | Condensation | Ethanol | DPV | 0.1 M Phosphate buffer (pH = 5) | 50 nM-10 μM | 10 nM |
| | MAA/EDMA/AIBN[70] | Chloroform | Heating at 60 ºC for 24 h | Methanol (Soxhlet extraction) | SWV | 0.07 M Hydrochloric acid | $1.7 \times 10^{-9}$- $9 \times 10^{-7}$ M | $5 \times 10^{-10}$ M |
| | Polyethylenediamine/ $SiO_2$/EGDMA[71] | - | Thermal polymerization for 8 h- | 0.1 M HCl | LSV | 0.1 M Phosphate buffer, (pH = 6.5) | 0.015-15 mg kg$^{-1}$ | 0.003 mg kg$^{-1}$ |
| | Chitosan[72] | Hydrochloric acid (pH< 6) | Potentiostatic at -1.1 V vs. SCE | Potentiostaticly at +0.6 V for 5 min 3 times, 0.01 M KCl | DPV | 0.1 M KCl | $10^{-7}$-$8 \times 10^{-5}$ M | $10^{-7}$ M |
| | MAA/ EGDMA/ AIBN[73] | $CHCl_3$ (for micro-sized MIP), MeCN (for nano-sized MIP) | Heating at 60 and 65 °C for 24 and 12 h for micro- and macrosized MIP, resp. | Methanol | SWV | 0.07 M Hydrochloric acid solution containing 12 % (v/v) of ethanol | 0.05 - 150 nM | 0.02 nM |
| | $(NH_4)_2TiF_6$/$H_3BO_3$/p-tert-butylcalix[4]arene[74] | Ethanol | Self-assembling | Ethanol | DPV | 0.1 M Phosphate buffer (pH 5) | $5 \times 10^{-8}$ - $1 \times 10^{-5}$ M | $1 \times 10^{-8}$ M |
| | Carmine[75] | 0.1 M Phosphate buffer (pH 6) | Potentiodynamic 1-2 V vs SCE | | CV and LSV | 0.1 M Phosphate buffer (pH 6) | $5 \times 10^{-8}$ - $1 \times 10^{-5}$ M | $1 \times 10^{-8}$ M. |

| Paraoxon | MAA/EGDMA/AIBN[7][8] | Chloroform | Heating at 65 ºC for 24 h | Methanol (Soxhlet extraction) | SWV | Acetate buffer (pH 5) | $3.8\times10^{-9}$- $7.5\times10^{-7}$ M | $10^{-9}$ M |
|---|---|---|---|---|---|---|---|---|
| Phoxim | Acrylamide/ ethylene glycol maleic rosinate acrylate/ AIBN[79] | Acetone | Heating at 60 ºC for 5 h | Methanol, acetic acid (7:3, v/v) | DPV | 0.05 M Acetate buffer (pH 6) | $8 \times 10^{-7}$ - $1.4 \times 10^{-4}$ M | $2 \times 10^{-8}$ M |
| Propazine | MAA/AA/4-vinyl pyridine/ EGDMA/ AIBN[80] | Toluene | Heating at 60 °C | Methanol, acetic acid (9:1, v/v) | DPV | 0.1 M Hydrochloric acid (pH 3) | 0.01–1 μM 1–55 μM | 0.001 μM |
| Rotenone | MAA/EDMA/AIBN/ styrene, $NaCl/K_2S_2O_8$/ dibutylphthalate/sodium dodecylsulfate /polyvinyl alcohol[81] | Dichloromethane | Heating at 65°C for 20 h | Acetic acid | DPV | Acetate buffer (pH 5.5) | 0.2–400 μg $L^{-1}$ | 0.1 μg $L^{-1}$ |
| Trans-resveratrol | AA/EGDMA/AIBN/ γ-methacyloxypropyl trimethoxysilane[82] | Acetonitrile | Heating at 55 °C for 24 h | CV (-0.2-1.2 V (36 cycles) | DPV | Phosphate buffer (pH 7.4) | $2\times10^{-6}$-$2\times10^{-5}$ M | $8\times10^{-7}$ M |
| Triazophos | o-hydroxyphenol/ $NaClO4$ (pH 5.5)[83] | 0.1 M Phosphate buffer (pH 7) | Potentiody-namic −0.6 - 1.2V vs Ag/AgCl | 0.5 M Sulfuric acid | CV | 0.1 M Phosphate buffer (pH 7), 0.1 M KCl | $2\times10^{-7}$ - $1\times10^{-5}$ M | $9.3\times 10^{-8}$ M |
| Triclosan | o-Phenylenediamine[84] | Acetate buffer (pH 5.2) | Potentiody-namic 0–0.8 V vs. SCE | 0.1 Sodium hydroxide | Ampero-metry | Acetate buffer (pH 5.2) or 0.01 M $K_4[Fe(CN)_6]$ soln. contg. 1 M $KNO_3$ | $2\times10^{-7}$-$3.0\times10^{-6}$ M | $8\times10^{-8}$ M |
| 2,4,6-Trichlorophenol | Methacrylamide/ 4-vinylpiridine/EGDMA/ AIBN/MWCNTs-COOH in $DMF-H_2O$[85] | Dimethylsulfoxide | Heating at 65 ºC for 24 h | Methanol with 15 % (v/v) acetic acid | DPV | 0.1 M Acetate buffer (pH 5) contg. $10^{-3}$ M $H_2O_2$ | Above $2.5\times10^{-5}$-$10^{-4}$ M | Above $2.5\times10^{-5}$ M |
| Trichlorfon | Tetraethylorthosilicate/ phenyltrimethoxysilane/methyltrimethoxysilane[86] | Ethanol | Sol–gel technology | Ethanol | CV | 2 M $K_3Fe(CN)_6$ contg. 0.05 M $KNO_3$ | $1\times 10^{-8}$- $1\times 10^{-6}$ g $mL^{-1}$ | $2.8 \times 10^{-9}$ g $mL^{-1}$ |
| Tolazoline | *o*-Aminothiophenol/ AuNPs[87] | Acetate buffer (pH 5.2) | Potentiody-namic -0.4 to +1.2 V vs. SCE | 0.2 M HCl | CV | 0.01 M Phosphate buffer (pH 6.8) contg. 0.1 M NaCl and 5 mM $K_3[Fe(CN)_6]$ | 0.05–5 μg $mL^{-1}$ 5–240 μg $mL^{-1}$ | 0.016 μg $mL^{-1}$ |

Abbreviations: 2,2′azobisisobutyronitrile(AIBN), Acrylamide (AA), Cyclic voltammetry (CV), Differential pulse adsorptive cathodic stripping voltammetry (DPAdCSV), Differential Pulse Voltammetry (DPV), Ethylene dimethacrylate (EDMA), Ethylene glycol dimethacrylate (EGDMA), Methacrylic acid (MAA), Square wave voltammetry (SWV), Trimethylolpropane tri methacrylate (TRIM)

## Conclusion

This review has focused on the molecular recognition of pesticides by synthetic receptors integrated with voltammetric transducers. Over the last 2 decades, great efforts have been done to combine MIP technology with electrochemical transduction. The majority of the sensor systems explored to date have used thermal polymerization including acrylic or vinylic monomers as recognition elements, but other phases (electrochemical polymerization, self- assembled monolayers, Sol-gel systems) have also been tested. Given the advantages of molecularly imprinted materials such as high stability, endurance, and low cost of production, it is plausible that products based on voltammetric sensors will reach the market soon.

## References

[1]Cooper, J., Dobson, H., (). *Crop Protect.*, **2007, *26*,** 1337.

[2]Sanborn, M., Kerr, K. J., Sanin, L. H., Cole, D. C., Bassil, K. L., Vakil, C. *Can. Family Physician*, **2007**, *53*, 1712.

[3]Aktar, W., Sengupta, D., Chowdhury, A., *Interdiscipl. Toxicol.*, **2007**, *2*, 1.

[4]Damalas, C. A., Eleftherohorinos, I. G., *Int. J. Environment. Res. Public Health*, **2011**, *8*, 1402.

[5]Alder, L., Greulich, K., Kempe, G., Vieth, B., *Mass Spectrom. Rev.*, **2006**, *25*, 838.

[6]Aulakh, J. S., Malik, A. K., Kaur, V., Schmitt-Kopplin, P., *Crit. Rev. Anal. Chem.*, **2005**, *35*, 71.

[7]Vagi, M. C., Petsas, A. S., Kostopoulou, M. N., Karamanoli, M. K., Lekkas, T. D., *Desalination*, **2007**,*210*, 146.

[8]Sherma, J., *J. Environ: Sci. Health, Part B.*, **2007**, *42*, 429.

[9]Ravelo-Pérez, L. M., Hernández-Borges, J., Rodríguez-Delgado, M. Á., *J. Sep. Sci.*, **2006**, *29*, 2557.

[10]Mathew, S. B., Pillai, A. K., Gupta, V. K., *Spectrochim. Acta Part A: Mol Biomol. Spectr.*, **2007**, *67*, 1430.

[11]Pacioni, N. L., Occello, V. N. S., Lazzarotto, M., Veglia, A. V., *Anal. Chim. Acta*, **2008**, *624*, 133.

[12]Moretto, L., Kalcher, K. (Eds.), *Environmental Analysis by Electrochemical Sensors and Biosensors: Fundamentals.* Springer, New York., **2014.**

[13]Janata, J., *Principles of Chemical Sensors.* Springer, New York., **2009**.

[14]Kounaves, S. P., in *Handbook of Instrumental Techniques for Analytical Chemistry*, F. A. Settle (Ed.), 709, Upper Saddle River, NJ: Prentice Hall PTR., **1997**.

[15]Vasapollo, G., Sole, R. D., Mergola, L., Lazzoi, M. R., Scardino, A., Scorrano, S., Mele, G., *Int. J. Mol. Sci.*, **2011**, *12*, 5908.

[16]Lee, S. W., Korposh, S., Selyanchyn, R., & Kunitake, T. (2012). Fundamentals and perspectives of molecular imprinting in sensor application. In S. W. Lee, & T. Kunitake (Eds.), *Handbook of molecular imprinting: advanced sensor applications* (pp.3-45). Boca Raton, FL: CRC Press.

[17]Ramström, O., Yan, M., in *Molecularly Imprinted Materials,* M. Yan, and O. Ramstron (Eds.), Marcel Dekker, New York, **2005**, 1

[18]Wulff, G., *Chem. Rev.*, **2002**, *102*, 1.

[19]Cheong, W. J., Yang, S. H., Ali, F., *J. Sep. Sci.*, **2013**, *36*, 609.

[20]Turiel, E., Martín-Esteban, A., *J. Sep. Sci.*, **2009**, *32*, 3278.

[21]Yilmaz, E., Schmidt, R. H., Mosbach, K., in *Molecularly Imprinted Materials*, M. Yan and O. Ramstron (Eds.), Marcel Dekker, New York, **2005**, 25.

[22]Holthoff, E. L., Bright, F. V., *Anal. Chim. Acta*, **2007**, *594*, 147.

[23]Yilmaz, E., Schmidt, R. H., Mosbach, K., In in *Molecularly Imprinted polymers. Man-made Mimics of Antibodies and Their Applications in Analytical Chemistry,* B., Sellegren (Ed.), Elsevier, Amsterdam, **2003**, 71.

[24]Kirsch, N. Whitcombe, M. J., in *Molecularly Imprinted Materials*, M. Yan, and O. Ramstron (Eds.), Marcel Dekker, New York, **2005**, 1.

[25]Andersson, L. I., Paprica, A., Arvidsson, T., *Chromatographia*, **1997**, *46*, 57.

[26]M*olecularly imprinted polymers: man-made mimics of antibodies and their application in analytical chemistry*, Sellergren, B. (Ed.), Elsevier, Amsterdam, **2000**, *23*.

[27]Ponton, A., Griesmar, P., Barboux-Doeuff, S., Sanchez, C., *J. Mater. Chem.,* **2001**, *11*, 3125.

[28]Tripathi, V. S., Kandimalla, V. B., Ju, H., *Sensors Actuators B: Chem*, **2006**, *114*, 1071.

[29]Mujahid, A., Lieberzeit, P. A., Dickert, F. L., *Materials*, **2010**, *3*, 2196.

[30]Niesen, T. P., De Guire, M. R., *Solid State Ionics*, **2002**, *151*, 61.

[31]Hishinuma, A., Goda, T., Kitaoka, M., Hayashi, S., Kawahara, H., *Appl, Surface Sci*, **1991**, *48*, 405.

[32]Masuda, Y., Kato, K., *J. Nanosci. Nanotechnol.*, **2009**, *9*, 439.

[33]Feng, L., Liu, Y., Hu, J., *Langmuir*, **2004**, *20*, 1786.

[34]Wang, C., Li, C., Wei, L., Wang, C., *Microchim. Acta*, **2007**, *158*, 307.

[35]Tatemichi, M., Sakamoto, M. A., Mizuhata, M., Deki, S., Takeuchi, T., *J. Am. Chem. Soc.*, **2007**, *129*, 10906.

[36]Sharma, P. S., D'Souza, F., Kutner, W., *Trends Anal. Chem.*, **2012**, *34*, 59.

[37]Ng, S. M., Narayanaswamy, R:, *Molecularly imprinted optical sensing receptors.* In: Lee, S. W., Kunitake, T., (Eds.) *Handbook of molecular imprinting advanced sensor applications*, Boca Raton, FL., CRC Press, **2012.**

[38]Sellergren, B., Rückert, B., Hall, A. J., *Adv. Materials*, **2002**, *14*, 1204.

[39]Tamayo, F. G., Titirici, M. M., Martin-Esteban, A., Sellergren, B., *Anal. Chim Acta*, **2005**, *542*, 38.

[40]Neto, J. D. R. M., Santos, W. D. J. R., Lima, P. R, Tanaka, S. M. C. N., Tanaka, A. A., Kubota, L. T., *Sensors Actuators B: Chem.*, **2011**, *152*, 220.

[41]Duan, Y., Luo, X., Zhang, H., Sun, G., Sun, X., Ma, H., *Analytical Methods*, **2013**, *5*, 6449.

[42]Tang, Q., Shi, X., Hou, X., Zhou, J., Xu, Z., *Analyst*, **2014**, *139*, 6406.

[43]Pardieu, E., Cheap, H., Vedrine, C., Lazerges, M., Lattach, Y., Garnier, F., Pernelle, C., *Analytica Chimica Acta*, **2009**, *649*, 236.

[44]Li, X., He, Y., Zhao, F., Zhang, W., Ye, Z., *RSC Advances*, 2015, *5*, 56534.

[45]Xie, C., Li, H., Li, S., Wu, J., Zhang, Z., *Analytical Chemistry*, **2009**, *82*, 241.

[46]Gholivand, M. B., Torkashvand, M., Malekzadeh, G., *Analytica Chimica Acta*, **2012**, *713*, 36.

[47]Zhao, L., Zhao, F., Zeng, B., *Int. J. Electrochem. Sci*, **2014**, *9*, 1366

[48]Du, D., Chen, S., Cai, J., Tao, Y., Tu, H., Zhang, A., *Electrochim. Acta*, **2008**, *53*, 6589.

[49]Xie, C., Gao, S., Guo, Q., Xu, K., *Microchim. Acta*, **2010**, *169*, 145.

[50]Guan, G., Wang, S., Zhou, H., Zhang, K., Liu, R., Mei, Q., Zhang, Z., *Anal. Chim. Acta*, **2011**, *702*, 239.

[51]Mazzotta, E., Malitesta, C., *Sensors Actuators B: Chem.*, **2010**, *148*, 186.

[52]Gómez-Caballero, A., Unceta, N., Goicolea, M. A., Barrio, R. J., *Sensors Actuators B: Chem.*, **2008**, *130*, 713.

[53]Wang, C., Li, C., Wang, F., Wang, C., *Appl. Surf. Sci.*, **2006**, *253*, 2282.

[54]Wong, A., Foguel, M. V., Khan, S., de Oliveira, F. M., Tarley, C. R. T., Sotomayor, M. D., *Electrochimica Acta*, **2015**, *182*, 122.

[55]Pellicer, C., Gomez-Caballero, A., Unceta, N., Goicolea, M. A., Barrio, R. J., *Analytical Methods*, **2010**, *2*, 1280.

[56]Toro, M. J. U., Marestoni, L. D., Sotomayor, M. D. P. T., *Sensors Actuators B: Chem.*, **2015**, *208*, 299.

[57]Kong, L., Jiang, X., Zeng, Y., Zhou, T., Shi, G., *Sensors Actuators B: Chem.*, **2013**, *185*, 424.

[58]Yan, X., Deng, J., Xu, J., Li, H., Wang, L., Chen, D., Xie, J., *Sensors Actuators B: Chem.*, **2012**, *171*, 1087

[59]Pan, M. F., Fang, G. Z., Liu, B., Qian, K., & Wang, S. *Anal. Chim. Acta*, **2011**, *690*, 175

[60]Basozabal, I., Gómez-Caballero, A., Unceta, N., Goicolea, M. A., Barrio, R. J., *Electrochim. Acta*, **2011**, *58*, 729

[61]Tan, X., Li, B., Liew, K., Li, C., *Biosensors Bioelectronics*, **2010**, *26*, 868.

[62]Tang, X., Zhang, D., Zhou, T., Nie, D., Yang, Q., Jin, L., Shi, G., *Anal. Methods*, **2011**, *3*, 2313.

[63]Li, H., Wang, Z., Wu, B., Liu, X., Xue, Z., Lu, X., *Electrochim. Acta*, **2012**, *62*, 319.

[64]Xue, X., Wei, Q., Wu, D., Li, H., Zhang, Y., Feng, R., Du, B., *Electrochimica Acta*, **2014**, *116*, 366.

[65]Zeng, Y., Yu, D., Yu, Y., Zhou, T., Shi, G., *J. Hazard. Mater.*, **2012**, *217*, 315.

[66]Zhang, D., Yu, D., Zhao, W., Yang, Q., Kajiura, H., Li, Y., Shi, G., *Analyst*, **2012**, *137*, 2629.

[67]Zhang, Y., Wu, L., Lei, W., Xia, X., Xia, M., Hao, Q., *Electrochimica Acta*, **2014**, *146*, 568.

[68]Luo, J., Cong, J., Liu, J., Gao, Y., Liu, X., *Anal. Chim. Acta*, **2015**, *864*, 74.

[69]Li, C., Wang, C., Wang, C., Hu, S., *Sensors Actuators B: Chem.*, **2006**, *117*, 166.

[70] Alizadeh, T., *Electroanalysis*, 2009, *21*, 1490.

[71]Yang, Q., Sun, Q., Zhou, T., Shi, G., Jin, L., *J. Agric. Food Chem.*, **2009**, *57*, 6558.

[72]Huang, Y. X., Lian, H. T., Sun, X. Y., Liu, B., *Chem. Res. Chin. Univ.*, **2011**, *27*, 28.

[73]Alizadeh, T., *Int. J. Environ. Anal. Chem.,* **2012**, *92*, 1742.

[74]Li, C., Wang, C., Wang, C., Hu, S., *Sensors Actuators B: Chem.*, **2006**, *117*, 166.

[75]Liu, X. Y., Li, C. Y., Hu, S., *Microchim. Acta*, **2006**, *154*, 275.

[76]Alizadeh, T., Ganjali, M. R., Norouzi, P., Zare, M., Zeraatkar, A., *Talanta*, **2009**,*79*, 1197.

[77]Guo, X., Zhou, H., Fan, T., Zhang, D., *Sensors Actuators B: Chem.*, **2015**, *220*, 33.

[78]Alizadeh, T., *Thin Solid Films*, **2010**, *518*, 6099.

[79]Tan, X., Wu, J., Hu, Q., Li, X., Li, P., Yu, H., Lei, F., *Anal. Methods*, **2015**, *7*, 4786.

[80]Gholivand, M. B., Malekzadeh, G., *Talanta*, **2012**, *89*, 513.

[81]Yang, M., Chen, Y., Ma, J., Huai, L., *Microchim. Acta*, **2009**, *166*, 95.

[82]Xiang, H. Y., Li, W. G., *Electroanalysis*, **2009**, *21*, 1207.

[83]Li, H., Xie, C., Li, S., Xu, K., *Colloids Surfaces B: Biointerfac.*, **2012**, *89*, 1751.

[84]Liu, Y., Song, Q. J., Wang, L., *Microchem. J.*, **2009**, *91*, 222.

[85]Diaz-Diaz, G., Blanco-López, M. C., Lobo-Castañón, M. J., Miranda-Ordieres, A. J., Tuñón-Blanco, P., *Electroanalysis*, **2011**, *23*, 201.

[86]Gao, W., Wan, F., Ni, W., Wang, S., Zhang, M., Yu, J., *J. Inorg. Organomet. Polym. Mater.*, **2012**, *22*, 37.0

[87]Zhang, J., Wang, Y., Lv, R., Xu, L., *Electrochim: Acta;* **2010**, 55, 4039.